AMT Discussions
"In situ observations of greenhouse gases over Europe during the CoMet 1.0 campaign aboard the HALO aircraft"
by Gałkowski et al.

Author's Response

Contents:

Note: Larger changes to the manuscript are marked under the appropriate responses to the reviewers' comments.

AMT-Discussions: Response to interactive review 1

Manuscript title: "In situ observations of greenhouse gases over Europe during the CoMet 1.0 campaign aboard the HALO aircraft", Gałkowski et al.
From: Anonymous Referee #1,
Review received and published: September 17th, 2020

Note: Original reviewer's remarks are given as ***bold and italicized text***. We've assigned each comment with a code for easier reference. Responses from authors are given below the comments.

RC 1.1. This paper presents a nice overview and synthesis of the two kinds of measurements made on the CoMet Aircraft, in-situ continuous and flask measurements, including isotopes. It also presents some analysis of the data, which in my view stretches a bit the goals for this journal, although I have definitely seen this type of thing before in AMT. The conclusion did a nice job of tying things together when really the results cover a lot of different topics, ranging from how well a global model reproduces vertical gradients to the isotopic value of the USCB. Very broad!

We thank the reviewer for this comment. Indeed, we spent quite some time thinking about the appropriate journal. We finally decided to put the measurement results at the core of our study. With this in mind, we thought that the demonstration of the usefulness of our measurements would fit our narrative, and comparison against widely-used state-of-the-art global models provided an excellent opportunity.

Other than that, it is well-written so I have very few editorial remarks below, and a few requests for more explanation of some of the measurement techniques, such as if and how water vapor was removed for the in-situ system.

Details:
RC 1.2. L69 ref to Varon is a satellite paper - this sentence reads as if it is a study using aircraft measurements.

We have moved the sentence in question to a paragraph discussing remote sensing techniques (after the text in L59).

RC 1.3. L94 should read "instruments"

Corrected.

RC 1.4. L115 tolerance

Corrected.

RC 1.5. L117 remove "so-called". I think working tanks is fine on its own.

Agreed.

RC 1.6. L121, were these two cylinders at different values?

Indeed, they were. We've added the information on the mole fractions of the calibration mixtures. Additionally, in L122, a minor correction regarding the length of calibration cycles was introduced. The respective fragment now reads:

"The instrument calibration was monitored during the mission with the use of two reference in-flight cylinders that contained dry mixtures of atmospheric air of known composition, for each tracer at a high and a low mole fraction, namely 373.4 -- 397.4 μmol mol^{-1} for CO_2, 1661.0 -- 1917.1 nmol mol^{-1} for CH_4, and 77.4 -- 139.5 nmol mol^{-1} for CO. These were analysed several times during each flight. The calibration cycle consisted of two intervals, each three minutes in length. The first minute of each interval was discarded in subsequent analyses due to pressure equilibration effects within the regulators."

RC 1.7. L 128, to be clear, the data itself was not adjusted for these in-flight calibration runs? Drift was assessed, was any drift found? If so, was it corrected? Why/why not? Were these in-flight calibrations noisier than expected so they were not used (see Karion et al., Long-Term Measurements of GHSs from Aircraft, AMT, 2013, for example)?

Indeed, in-flight calibrations were used exclusively to monitor for drifts. No significant drift was found. The flight-to-flight variation of each low- and high-span measurement during the period prior to the instrument malfunction on June 7th was slightly larger than expected for CO_2, but not for other gases.

We added the following paragraph to the result section (3.1, approx.. L266 in the revised manuscript) of the manuscript, describing this in more detail:

"Results from in-flight measurements of the two reference cylinders showed no significant drift, however the flight-to-flight variation of each low- and high-span measurement during the period prior to the instrument malfunction on June 7th was slightly larger than expected for CO_2: low-span measurements varied by 0.10 μmol mol^{-1}, 0.4 nmol mol^{-1}, and 1.0 nmol mol^{-1}, while high span measurements varied by 0.14 μmol mol^{-1}, 0.3 nmol mol^{-1}, and 0.8 nmol mol^{-1} for CO_2, CH_4 and CO, respectively. The likely cause for this are the silicon rubber membranes used in the pressure regulators (Filges, 2015), which are known to cause diffusion of CO_2 (Hughes, 1995). Given that species other than CO_2 did not show unexpected behaviour, we did not apply any correction of the measurements resulting from the in-flight measurements of the reference cylinders. For this reason, we also did not apply any correction of drift within each flight, in contrast to the experience of Karion et al. (2013b).

RC 1.8. Was the sample dried prior to measurement by the Picarro? If so, does the calibration gas also pass through the drying system? If not, how was the effect of water vapor removed?

The sample was not dried externally. The water correction was performed based on online measurements of H_2O and followed the procedure described by Filges et al. (2015), which is

consistent with a more recent study from Reum et al. (2019). We have added this information in section 2.2.1. (after L118 in the revised manuscript). It reads:

"The instrument reports dry mole fractions, defined as number of molecules of each species in moles per one mole of dry air, with typical observed ranges expressed in µmol mol^{-1} for CO_2 (equal to one part per million, ppm) and in nmol mol^{-1} for CO and CH_4 (equal to 1 part per billion, ppb). As the collected air was not dried in the sampling line, a water correction was applied based on the online measurements of H_2O mole fraction, following the approach described in previous studies of Filges et al. (2015) and Reum et al. (2019).

RC 1.9. Somewhere in Sec 2 should be mentioned the quantity being measured, i.e. the dry air mole fraction of the species, with the definition that it is the moles of the species per mole of dry air, and define ppm as parts per million, or micromoles of CO2 per mole of dry air... etc. These are formalities but they are useful so we keep the work accessible and clear.

We have added the short definition in subsection 2.2.1. together with the information on water correction (c.f. RC 1.8. above).

RC 1.10. L145-155, and throughout. Units should all be in metric, I see a lot of inches (") here. Inches I believe should be abbreviated as in. Perhaps give in cm with inches in parentheses?

Agreed, now OD given in mm with inches in parentheses.

RC 1.11. L169- how was this drift discovered, was it by comparing the flask analysed value from the lab with the in-situ system during flight? How big is "significant" (curious)?

The first occurrence of the issue was observed when comparing the flask values against corresponding in situ observations done with JIG. Mean bias between these two was equal to -9.4 $\pm$ 1.2 nmol mol^{-1} for flights 1—7 and -11.0 $\pm$ 2.6 nmol mol^{-1} for flights 8—9, much larger than expected. For several flask samples analysis repetitions were made after a few days that yielded systematically higher CO results (1.5 – 3 nmol mol^{-1} within 2 – 20 days indicating drift rates of up to 1 nmol mol^{-1} d^{-1}.

To find the reason for that discrepancy, we have analysed flasks that were not filled during the campaign, which still contained the conditioned air samples from Jena. As the GasLab at MPI-BGC carefully maintains the mole fractions of these conditioning mixtures, we were able to diagnose that indeed the CO values of these flasks were drifting.

Following on these initial results, a lab experiment was performed in early 2019, where 10 flasks were equipped with different configurations of the sealing caps. One of the flasks tested was equipped with the same type of sealing caps as the flask set used during CoMet (namely 7 PCTFE type). It was found that for this type of cap the drift in CO was significantly larger than for those of the regular flask pool used in other field measurements supported by GasLab in Jena (about 2.9 nmol mol^{-1} $month^{-1}$ per cap). No extra effect was observed for other gases.

As the exact reason behind this extra drift couldn't be established, and a precise correction function could not be calculated, we have decided to discard the CO measurements.

We have added some of the extra information to the manuscript in section 2.2.2:

"A significant (approximately 10 nmol mol^{-1}) bias in CO mole fractions was observed when comparing in situ measurements from JIG against gas flasks collected using JAS. Control laboratory experiments run after the campaign have shown that this bias was a result of a growth in CO mole fractions in the period between sample collection and subsequent laboratory analysis. This enhancement of the mole fraction could be attributed to new valve sealing polymer but could not be accurately corrected, therefore we have decided to discard these results. Careful quality control and additional tests did not show any sign of other gases being affected."

RC 1.12. L258: first time a broken mounting is mentioned, earlier it is referred to a roll-out malfunction. Perhaps either give a little detail or keep referring to it as a malfunction? I think a sentence would be nice as to what happened exactly?

Thank you for pointing this out. Detailed description of the malfunctions is given in L134-141. The text (L288 in the revised manuscript) has been clarified and now reads:

"After the malfunction (see section 2.2.1.), i.e. for flights no. 8 and 9, these mean offsets were equal to 0.127 (68) μmol mol^{-1} and -0.64 (91) nmol mol^{-1} for the respective gases. While the difference of values as compared to flights 1--7 is statistically significant, it is still close to the WMO compatibility goal.

RC 1.13. L289 and elsewhere, I would think approximately should be spelled out.

Agreed.

RC 1.14. L300 and Section 3.4: I am starting to wonder if AMT is the appropriate forum for his extensive model-data comparison, as we are moving well beyond measurement techniques here.

We thank the reviewer for this remark. Partial answer to that question has been given already in our comment to the initial statement (RC 1.1.).

We would like to further underline that our intention in sections 3.2 – 3.4 was primarily to use the models to assist in interpreting the collected measurements. Thanks to that, we believe we can simultaneously:

a) Further increase the confidence in our measurement results (e.g. when observing positive or negative peaks in both the model and observations we can with more certainty assume that this is due to large– or regional–scale physical processes rather than equipment issues or local effects)
b) Better understand the causes behind the observed signals which would then allow us and scientific community in general to improve the measurement strategies for the future campaigns.

These goals can only be achieved if we can trust in the model results, hence a more detailed discussion was necessary. Perhaps the model comparisons included in sections 3.3 and 3.4 might not directly be related to measurement techniques, but we have decided to use this opportunity and expand the discussion, as we believe a mutual benefit for both modelling and observational communities could be thus achieved.

RC 1.15. Fig 8 These are impressive 3D renderings - this kind of data is difficult to visualize. But I am a little lost - if the plots on the right correspond with the flights on the left, then why are there more points in the Miller-Tans plots than on the left (i.e. the lower should only have 4 points then correct?). Something I am missing here?

Thank you for that comment. Miller-Tans plot on the right is done using a combined sample set from both flights shown on the left. We have excluded samples collected in higher layers of the atmosphere (above 3 km altitude), as we assumed that they represent an airmass of different origin due to large-scale transport phenomena. Based on the wind analyses and supporting modelling results we assume that we can aggregate both sample sets and treat them as representative of a mean source from the USCB. This is stated in L424-427. Two panels on the Miller-Tans plot are not plotted separately for two measurement days, but present δ^2H and $\delta^{13}C$ values measured in the combined dataset, i.e. each panel contains eight observation.

We have modified the caption of Fig. 8 for further clarification, and also added "data combined" in the panel label We have also corrected a minor mistake in the data subset description: the altitude threshold for flasks used in Miller-Tans plots was previously given as 4 km; the correct value is 3 km.

The new caption now reads:

"Left: Visualisation of CH_4 measurements over USCB during flights no. 6 (a) and no. 7 (b). For flight no. 7, only data from below 4 km altitude is plotted for clarity. Coloured lines represent mole fractions along the flight path, with the first plotted measurement marked with 'x', triangles show the flask sampling locations. Both in situ and flask mole fractions are coloured using the same scale. c) Miller-Tans model of isotopic source signatures for δ^2H and $\delta^{13}C$, based on eight flask samples collected below 3 km over the USCB during flights no. 6 and 7 together. See text description for details. The dashed line is the linear fit calculated using the Williamson-York formula (Cantrell, 2008). Values of fit parameters are given with 1-σ uncertainty in the parentheses".

References added to the revised manuscript:

Karion, A., Sweeney, C., Wolter, S., Newberger, T., Chen, H., Andrews, A., Kofler, J., Neff, D., and Tans, P.: Long-term greenhouse gas measurements from aircraft, Atmospheric Measurement Techniques, 6, 511–526, https://doi.org/10.5194/amt-6-511-2013,

Reum, F., Gerbig, C., Lavrič, J.V., Rella, C.W., Göckede, M., 2019. Correcting atmospheric CO2 and CH4 mole fractions obtained with Picarro analyzers for sensitivity of cavity pressure to water vapor. Atmos. Meas. Tech. 12, 1013–1027. doi:10.5194/amt-12-1013-2019

AMT-Discussions: Response to interactive review 2

Manuscript title: "In situ observations of greenhouse gases over Europe during the CoMet 1.0 campaign aboard the HALO aircraft", Gałkowski et al.
From: Anonymous Referee #2,
Review received and published: September 22nd, 2020

Note: Original reviewer's remarks are given as ***bold and italicized text***. We've assigned each comment with a code for easier reference. Responses from authors are given below the comments.

General Comments

RC 2.1. ***The manuscript presents a broad overview and analysis of results of aircraft in situ measurements (continuous greenhouse and trace gases) and atmospheric trace gas and isotopic composition measurements in onboard flask samples conducted during the CoMet 1.0 campaign. It details these two measurement systems and inter-comparisons in the context of WMO compatibility goals and presents model-data comparisons to two commonly used global modelling systems with different resolutions and meteorological drivers. The article is well written, concise, and scientifically sound, but I feel that the focus of this manuscript stretches the limits of the scope of the AMT journal. As such, and since the article is part of a special issue collection, the majority of my specific comments aim to provide more detail for important measurement techniques below.***

We thank the reviewer for that comment. As explained in our reply to reviewer #1, we are aware that some sections of our manuscript might be on the edge of the scope for AMT. We believe, however, that including some analysis of the measurements is beneficial for our manuscript and improves the overall value of the paper for the general scientific community.

We kindly refer the referees to our previous discussion of above (see RC 1.1. and RC 1.14.).

Specific Comments

RC 2.2. Section 2.2.1 describes the CRDS measurements, but there is some key information and clarification lacking from the description of this system and its operation that should be included here. For example, air sample drying and/or water vapour corrections to these greenhouse gas measurements should be discussed as these measurements are compared to dried flask sample measurements.

We kindly refer to section RC 1.8. in this document.

RC 2.3. Furthermore, 'mixing ratios' measured should be reported as dry air mole fractions: please replace 'mixing ratio' with 'mole fraction' throughout the text.

Agreed, units have been replaced as requested. See also our discussion in RC 1.9.

RC 2.4. It would also be useful to also specify how many in-flight offset-corrections occurred on average per flight as these were performed manually, and specify whether this is a single-point correction or if two calibration tanks were used.

We thank the reviewer for these remarks. We have taken them into the account when addressing point RC 1.7. See discussion there.

RC 2.5. For flask samples, please clarify the level to which air samples are dried with the magnesium perchlorate and the pressure and volume of air that is sampled in each glass flask (is this 1 L at ambient pressures?).

The air is dried to dew points below -70 °C. With regard to the pressure inside flask, the following text was modified in section 2.2.2. at approx. L159:

"(…) that provides the over-pressure necessary to flush and pressurise the flasks, up to approximately 1500 hPa."

RC 2.6. On which type of analyser were the flasks measured?

The description of the measurement instruments was expanded in section 2.2.2.:

"Gas chromatographic analysis of air in glass flasks is made with a gas chromatographic system based on two GCs (6890A, Agilent Technologies) equipped with a flame ionisation detector and a Nickel CO_2 converter (FID) for CH_4 and CO_2, an electron capture detector (ECD) for N_2O and SF_6, a helium ionisation pulsed discharge detector (D-3-I-HP, Valco Instruments Co. Inc.) for H_2, and a HgO Reduction Gas Analyser (RGA3, Trace Analytical) for H_2 and CO. Additional analyses of O_2/N_2, Ar/N_2 and isotopic composition of methane $\delta^{13}C$ -CH_4 and $\delta^{2}H$ -CH_4 were carried out in the IsoLab of MPI-BGC (Sperlich et al., 2016). The typical measurement precision of the laboratory analyses is given in Table 1."

RC 2.7. L169 states that there was a drift in the CO flask measurements between collection and measurement; for clarity, please elaborate on how you have determined this using the in situ data.

Description has been expanded following the discussion of RC 1.11 here – we kindly refer to the discussion above.

RC 2.8. L194: Please also clarify how flasks were sampled during vertical profiles; if the aircraft was only either ascending/descending over the flask fill time, the reader can infer that the air samples collected during these profiles represents an integrative mole fraction between potentially several layers of the atmosphere. It might therefore also be useful to state, on average, how long it takes to fill a flask.

Indeed, the filling time was variable with height. The altitude to which the flask was assigned to was assigned based on the box model that took into the account flow, pressure and tubing volumes, as

described in L159-L163, following the work of Chen et al. 2012. We've added the following additional information into the text after 170:

"Each flask was flushed with 10 times its volume prior to closing the upstream and downstream valves. Typically, flasks were filled during descending profiles, but on some occasions also during ascents. The variable ambient pressure caused the flask fill time to vary between 100 seconds at high altitudes to 25 seconds close to the surface."

RC 2.9. Throughout the manuscript, the Jena CarboScope model is referred to as TM3, but in L235, it is mentioned that it will be referred to as "CarboScope" – please choose one or the other for consistency.

The plots and captions have been updated and now use CSc in place of TM3.

RC 2.10. It is mentioned in Section 4 that the flask measurements are compatible, by WMO standards, with the G2401 measurements but this does not seem to be the case. The in situ-flask differences, given uncertainties, fall outside of WMO surface compatibility goals for CO2 (0.1 ppm) and CH4 (2 ppb). As compatibility between measurement systems is mentioned as one of the scientific goals of the CoMet 1.0 mission, it seems necessary to state these compatibility goals for CO2 and CH4 as defined by WMO.

Thank you for this remark. In line 257 we have stated that the results are the difference is "still close to the WMO compatibility goal". However, the later statement in the "Conclusions" section was incorrect. This has been changed into (L508):

"Comparison with flask samples analysed in the laboratory confirm that the measurement data are close to compliance with the WMO compatibility goals (average bias smaller than 0.15 μmol mol^{-1} and 3 nmol mol^{-1} for CO_2 and CH_4, respectively)"

We have added the requested information on WMO compatibility goals in L285:

"The comparison between flask and in situ measurements is available for all except one flight (no. 5). From the 96 samples collected and analysed, 84 had simultaneous in situ measurements available from JIG that could be used for a bias assessment. Here, we compare bias between both our datasets to the 'network compatibility goal', defined by World Meteorological Organization as "the scientifically-determined maximum bias among monitoring programmes that can be included without significantly influencing fluxes inferred from observations with models" (WMO, 2019). WMO specifies this compatibility goal as equal to 0.1 μmol mol^{-1} for CO_2 (in the northern hemisphere) and 2 nmol mol^{-1} for both CH_4 and CO."

RC 2.11. Figure 3 does not define the differences shown (i.e. are flask – in situ values shown)? I also wonder why these results are shown by flight number rather than something more informative for understanding differences between the two systems (e.g. difference vs. altitude or difference vs. mole fraction), separating flights 1-7 and 8-9. I would suggest a figure showing these differences as a function of either of these parameters (perhaps in SI) to shed light on why differences are seen between in situ and flask greenhouse gases.

In the course of data analysis, we have investigated the mismatch between JIG and JAS in detail and found no clear relationship of in situ vs. flask mole fractions with either altitude or mole fraction (see figures below).

For both CO_2 and CH_4, the distribution of difference seems to be largely independent of altitude (Fig. A). Three outliers with very negative bias for methane (below 10 nmol mol^{-1}) are observed around 10 km, however even for high altitudes most of the differences are in the typical reported range (approximately -5 to 0 nmol mol^{-1}, with the mean of -2.93, nmol mol^{-1}).

As shown in Fig. B., the variability of JIG-JAS difference seems to be slightly higher closer to the higher end of the observed mole fraction range, however no clear trend can be observed. For methane, small biases are observed in the lower mole fraction ranges (below 1850 nmol mol^{-1}) with outliers for very low values of methane seemingly less biased than the ones observed in the typical tropospheric range (1900-1950 nmol mol^{-1}).

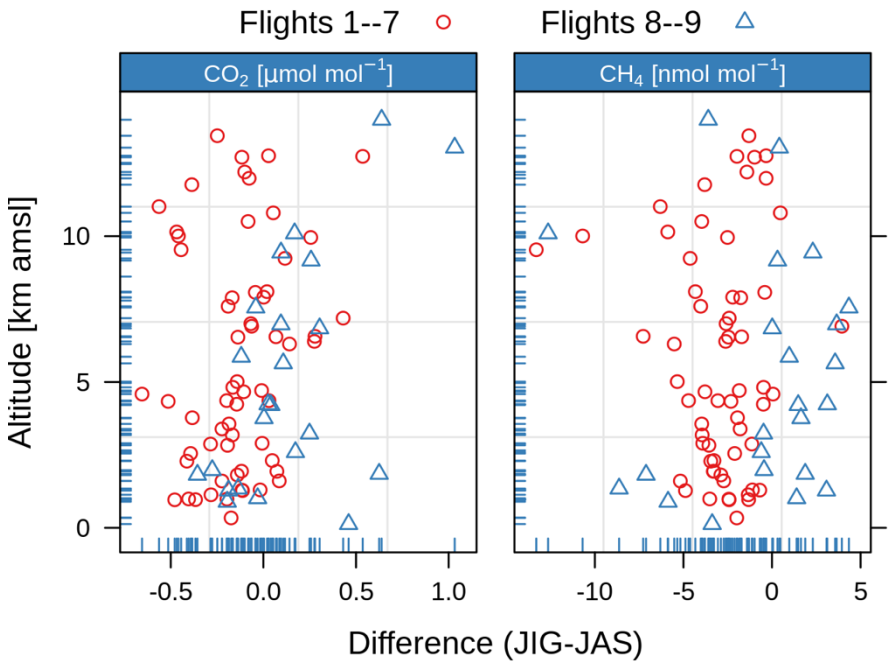

Figure A. Difference between JIG in situ and flask values, and their dependence on altitude, presented separately for flights 1—7 (red) and 8—9 (blue). Notches added to X and Y axes to display distribution of values (these are not colour-labeled).

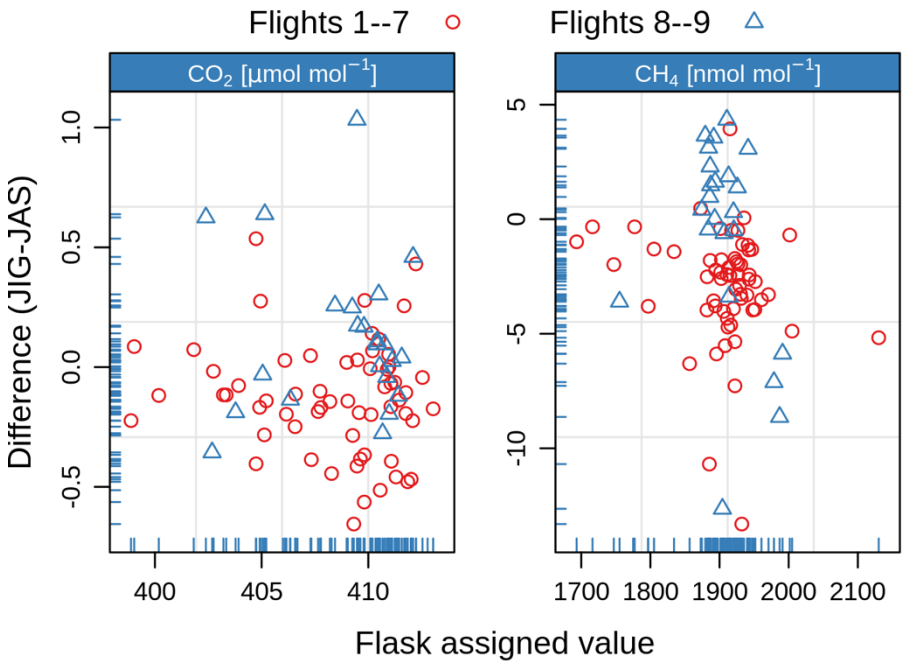

Figure B. Difference between JIG in situ and flask values plotted as a function of mole fractions. Notches were added to X and Y axes to display the distribution of values (notches are not colour-labeled).

We've therefore decided that we want to emphasize first and foremost the change in the mean offset in flights 8—9, and to present the day-to-day variability, which is done in Figure 3 of the manuscript.

The plot has been updated in the following manner: i) difference is now clearly defined with the Y label axis; ii) units changed to µmol mol^{-1} and nmol mol^{-1} for CO_2 and CH_4, respectively, for consistency with the rest of the text (c.f. RC 2.3).

RC 2.12. L290: Please describe how it was evidenced that a stratospheric intrusion was crossed.

'Stratospheric intrusion' in this sentence is meant to describe stratospheric air being pulled below typically observed altitude ranges. This is supported by comparison of CAMS model predictions and our in situ observations for all greenhouse gases (Fig. 4), where we see a clear segment of airmass with significantly reduced mole fractions, which is probably a potential vorticity (PV) filament that has been brought down by the outflow of the convective system. While we did not measure the ozone concentrations that are typically associated with stratospheric intrusions, and the observed air mass clearly doesn't reach deep into the troposphere, we believe that the very high correlation between observations and the model allows us to identify the phenomenon by stratospheric air presence at the flight level.

The text at L290 has been expanded, with stratospheric intrusion changed to 'stratospheric filament' in order to prevent confusion with the dry intrusions associated with large-scale tropopause folds:

"Immediately before the descent to Monte Cimone it crossed a stratospheric air filament, possibly brought down to the flight level by the outflow of a deep convective system active in the area in the afternoon on that day. This is corroborated by CAMS model results, which show a clearly

defined air-mass structure, depleted in mole fractions for all the observed compounds, stretching from the stratosphere at 200 hPa down to approximately 400 hPa (corresponding to roughly 13 km and 8 km a.m.s.l., respectively)."

RC 2.13. Figure 4, at times (L292, and elsewhere) is described in kilometers, but the figure itself is denoted in pressure altitude. The text would be more consistent with this figure if it were describing events in pressure levels as well.

Agreed. The text has been updated to use pressure levels together with altitudes.

RC 2.14. Figure 5 shows modeled vertical profiles, which seems redundant with Figure 6. In addition, these model vertical profiles are not ever discussed. I would suggest removing these panels.

We respectfully disagree. We believe that showing modelled profiles also in Fig. 5. gives a one-look visual comparison as to the nature of model vs. observation difference that would require careful, simultaneous analysis of both figures by the reader. Additionally, it also allows one to identify the distinct differences between CarboScope and CAMS products at the profile locations.

Technical Corrections:

RC 2.15. L14: Uncertainties are given in parentheses and not quotes, please rephrase.

Corrected.

RC 2.16. L83: Please define 'HALO' if this is an acronym

Agreed. Also defined in the abstract.

RC 2.17. L101: G4201-m should be G2401-m, I believe.

2.17. Indeed. We thank the reviewer for pointing this out.

RC 2.18. L101: 'fulfil' is missing ans 'l'

'Fulfil' is an acceptable form, used primarily in British English. (Oxford Advanced Learner's Dictionary, 7th Edition). We have left it as is.

RC 2.19. *L115: Please change 'tollerance' to '*tolerance'

Corrected.

RC 2.20. *L200: Please change to 'boundary'*

Corrected.

RC 2.21. L222: Please eliminate "when possible" and "when not"

Sentence now reads:

"In order to estimate the background signature, we have used measurements from air samples collected in the immediate vicinity of the target plume, either from the upwind air masses or from outside of the main plume."

RC 2.22. L244: Change 'these' to 'and'

Modified sentence now reads:

"Data from 51 vertical profiles are available, out of which 21 have simultaneous flask measurements. They are listed in the supplement (Table S1)."

RC 2.23. L253: Change 'brackets' to 'parentheses'

Corrected.

RC 2.24. Figure 2 caption: please define what red/blue shading means. Black crosses are hard to see – perhaps a thicker line would suffice. Altitude should be specified as km ASL.

The caption was updated according to reviewer's suggestions. The plot was also updated, with the crosses now 20% thicker and 20% larger; a small black dot was added in the centre on the top of the observations (blue line) to exactly define the value for 12.06.2018, where some of the crosses are largely covered by the data series. The width of the blue line was reduced by 30% to further make the crosses more visible. Similar changes were applied to Figure S2.

RC 2.25. L273-275 might be more easily understood if (a)-(d) were noted on Figure 4.

Agreed.

The plot has been updated in the following manner: i) markings for periods a—d were added to the bottom three panels of the plot; ii) units have been changed to mole fractions, consistent with the rest of the manuscript; iii) vertical coordinate label switched to hPa. Caption and manuscript have been adjusted accordingly.

RC 2.26. Figure 5 denotes CH4/CO/CO2 mole fractions as 'X[ ]', which is somewhat mis-leading as XCH4/XCO/XCO2 typically denote total-column mole fractions.

We have used a Greek letter χ, which has been used before (instead of c) to denote mole fractions. See e.g. Röckmann et al., 2016. Similar notation was also used in Karion et al., 2013. This has been left as is.

RC 2.27. L369-370: The offsets in the 3-10 km range are actually responsible for the tail.

We have clarified the description:

“Interestingly, the distribution of the mismatch in this altitude range is a positively skewed Gaussian curve (Fig. 6, bottom-right panel), with the values in the main peak almost symmetric around 0 µmol mol^{-1}, and the mean offset in the 3 – 10km range driven by the values in the tail of the distribution.”

RC 2.28. ***Figure 8 caption “For flight no. 7 on the four flasks…” (plural)***

No longer relevant, as this caption has been modified following to RC 1.15.

RC 2.29. ***Figure S2: Please increase line width for purple crosses, as these are difficult to see.***

Figure S2 was updated similar to figure 2 (see RC 2.24 above). The label “TM3” was also replaced with Carboscope / CSc for consistency. The caption was updated accordingly.

References added to the revised manuscript:

Sperlich, P., Uitslag, N. A. M., Richter, J. M., Rothe, M., Geilmann, H., van der Veen, C., Röckmann, T., Blunier, T., and Brand, W. A.: Development and evaluation of a suite of isotope reference gasesfor methane in air, Atmospheric Measurement Techniques, 9, 3717–3737, https://doi.org/10.5194/amt-9-3717-2016, https://www.atmos-meas-tech.net/9/3717/2016/, 2016

In situ observations of greenhouse gases over Europe during the CoMet 1.0 campaign aboard the HALO aircraft

Michał Gałkowski[1,2], Armin Jordan[1], Michael Rothe[1], Julia Marshall[1*,5], Frank-Thomas Koch[1,3], Jinxuan Chen[1], Anna Agusti-Panareda[4], Andreas Fix[5], and Christoph Gerbig[1]

[1]Department of Biogeochemical Systems, Max Planck Institute for Biogeochemistry, Jena, Germany
[2]Faculty of Physics and Applied Computer Science, AGH University of Science and Technology, Kraków, Poland
[3]Meteorological Observatory Hohenpeissenberg, Deutscher Wetterdienst, Germany
[4]European Centre for Medium-Range Weather Forecasts, Reading, UK
[5]Deutsches Zentrum für Luft- und Raumfahrt (DLR), Institut für Physik der Atmosphäre, Oberpfaffenhofen, Germany
[*]former affiliation

Correspondence: Michał Gałkowski (michal.galkowski@bgc-jena.mpg.de)

Abstract.

The intensive measurement campaign CoMet 1.0 (Carbon dioxide and Methane mission) took place during May and June 2018, with a focus on greenhouse gases over Europe. CoMet 1.0 aimed at characterising the distribution of CH_4 and CO_2 over significant regional sources with the use of a fleet of research aircraft, as well as validating remote sensing measurements from state-of-the-art instrumentation installed on-board against a set of independent in-situ observations. Here we present the results of over 55 hours of accurate and precise in situ measurements of CO_2, CH_4 and CO ~~mixing ratios~~ mole fractions made during CoMet 1.0 flights with a cavity ring-down spectrometer aboard the German research aircraft HALO (High Altitude and LOng Range Research Aircraft), together with results from analyses of 96 discrete air samples collected aboard the same platform. A careful in-flight calibration strategy together with post-flight quality assessment made it possible to determine both the single measurement precision as well as biases against respective WMO scales. We compare the result of greenhouse gas observations against two of the available global modelling systems, namely Jena CarboScope and CAMS (Copernicus Atmosphere Monitoring Service). We find overall good agreement between the global models and the observed ~~mixing ratios~~ mole fractions in the free-tropospheric range, characterised by very low bias values for the CAMS CH_4 and the CarboScope CO_2 products, with a mean free tropospheric offset of 0 (14) $\mathrm{nmol\,mol^{-1}}$ and 0.8 (1.3) $\mathrm{\mu mol\,mol^{-1}}$ respectively, with the ~~quoted number~~ numbers in parentheses giving the standard uncertainty in the final digits for the numerical value. Higher bias is observed for CAMS CO_2 (equal to 3.7 (1.5) $\mathrm{\mu mol\,mol^{-1}}$), and for CO the model-observation mismatch is variable with height (with offset equal to -1.0 (8.8) $\mathrm{nmol\,mol^{-1}}$). We also present laboratory analyses of air samples collected throughout the flights, which include information on the isotopic composition of CH_4, and we demonstrate the potential of simultaneously measuring $\delta^{13}C-CH_4$ and $\delta^{2}H-CH_4$ from air to determine the sources of enhanced methane signals using even a limited amount of discrete samples. Using flasks collected during two flights over the Upper Silesian Coal Basin (USCB, southern Poland), one of the strongest methane-emitting regions in the European Union, we were able to use the Miller-Tans approach

to derive the isotopic signature of the measured source, with values of δ^2H equal to -224.7 (6.6) ‰ and δ^{13}C to -50.9 (1.1) ‰, giving significantly lower δ^2H values compared to previous studies in the area.

1 Introduction

Increased ~~mixing ratios~~ mole fractions of atmospheric greenhouse gases (GHGs) are recognised as the primary cause of the warming observed in the climate system over the past 70 years. Of these, the most important are carbon dioxide (CO_2) and methane (CH_4), respectively responsible for approximately 56 % and 32 % of the globally-averaged increase in radiative forcing caused by greenhouse gases, as compared to the pre-industrial period (IPCC et al., 2013). Further increases in the atmospheric burden of greenhouse gases are expected to lead to a multitude of negative impacts over a wide range of climate system components throughout the 21st century and beyond. These include further temperature increase, sea level rise, changes in precipitation patterns, shrinking of ice cover and more. Furthermore, cumulative emissions of CO_2 will have lasting effects on most aspects of climate for many centuries, even if anthropogenic emissions are stopped altogether (IPCC et al., 2013).

The accuracy of climate projections is substantially reduced, however, by uncertainties in the specific components of greenhouse gas budgets, which stem either from difficulties in precise estimation of direct sinks and emissions, or from our limited understanding of specific feedback processes. Despite the critical importance of this issue, our knowledge about even the two most important anthropogenically-influenced greenhouse gases, CO_2 and CH_4, is still inadequate. In fact, even though intense scientific and political activities have targeted this area of research over the past 20 years, the uncertainties related to the most important source and sink processes remain high (Ballantyne et al., 2015), reflecting the enormous complexity of the Earth System, with its multitude of elements and feedback mechanisms, operating on a vast range of spatial and temporal scales.

Main sources of uncertainties in the reported budgets are similar for both CO_2 and CH_4. When considering bottom-up methods, they are related either to a) the lack of representativeness of flux measurement sites used for up-scaling the fluxes from specific source areas, or b) incomplete knowledge at the process level, which affects the emission models used for the calculation of either emission factors or actual fluxes. Top-down methods, in turn, are based on inverse modelling and critically depend on the availability of high-precision atmospheric observations in the areas studied, which is still insufficient. In order to significantly reduce the global uncertainties in the budgets of greenhouse gases using ground-based instrumentation, a significant expansion of the observation networks is required to provide precise regional budgets for the most important source and sink areas (Ciais et al., 2014). Observation networks of sufficient density are currently only available over Europe and parts of North America, where they have been used successfully to constrain anthropogenic and biogenic fluxes of greenhouse gases (e.g. Bergamaschi et al., 2018).

Utilising space-borne observations can bridge the data gap by providing high-resolution data on regional scales across the globe, which has driven significant developments in remote sensing techniques since the mid-1990s. Since the launch of SCIAMACHY in 2002, remote sensing data on global distributions of column-averaged dry-air ~~mixing ratios~~ mole fractions for atmospheric carbon dioxide (XCO_2) and methane (XCH_4) comes most often from surface-reflected near- and short-wave infrared radiation detectors (Bovensmann et al., 1999; Kuze et al., 2009; Reuter et al., 2011; Butz et al., 2012; Eldering et al.,

2012; Reuter et al., 2019). While important insights into greenhouse gas budgets have been gained (Bergamaschi et al., 2013; Basu et al., 2013), there are still significant limitations when using infrared methods (Kirschke et al., 2013; Le Quéré et al., 2018). As an alternative to passive remote sensing, the Integrated Path Differential Absorption (IPDA) technique has been adapted in recent years to provide column-averaged measurements of greenhouse gas ~~mixing ratios~~ mole fractions with high accuracy ~~(e.g. Amediek et al., 2008; Sakaizawa et al., 2009; Spiers et al., 2011; Dobler et al., 2013; Du et al., 2017; Amediek et al., 2017)~~ (e.g. Amediek et al., 2008; Sakaizawa et al., 2009; Spiers et al., 2011; Dobler et al., 2013; Du et al., 2017; Amediek et al., 2017) . All of these remote sensing techniques rely heavily on the availability of independent calibration and validation data sets. A good overview on how remote sensing observations can be used to infer fluxes is presented in Varon et al. (2018).

Aircraft measurements are flexible and constitute a critical link for bridging the gap between ground-based networks and space-borne observations in constraining emissions at multiple scales. They can be performed either with precise in situ measurement techniques that can be calibrated and made traceable to WMO calibration scales (e.g., Wofsy, 2011; Sweeney et al., 2015; Filges et al., 2018; Boschetti et al., 2018; Umezawa et al., 2018) or utilizing remote sensing instruments (Krings et al., 2013). Airborne observations can be applied to describe regional and local variability of the observed signals (Wofsy, 2011; Sweeney et al., 2015). They can also be used as validation of the coupled transport-emission models (Ahmadov et al., 2007; Sarrat et al., 2007; Park et al., 2018; Leifer et al., 2018), or used to directly infer the fluxes of measured components. Such direct inference has been demonstrated in the past, e.g. using Gaussian plume models (Krings et al., 2013), Lagrangian mass-balance approaches (Karion et al., 2013a; Cambaliza et al., 2014) or regional Bayesian inverse-modelling systems (e.g.: Saeki et al., 2013; Boschetti et al., 2018). ~~Other techniques of flux estimation also exist (c.f. Varon et al., 2018).~~

In order to further push the limits and improve the observation and modelling methods developed in the past, a multi-platform aircraft research mission was envisaged, designed, proposed and executed in collaboration between the German Aerospace Center (DLR), the Max Planck Institute for Biogeochemistry (MPI-BGC), the University of Bremen, the Free University of Berlin, AGH University of Science and Technology, and other partners. CoMet 1.0 (Carbon Dioxide and Methane Mission, see the overview paper by Fix et al. in this Special Issue), executed in May and June 2018, targeted hot-spots of CO_2 and CH_4 emissions in Europe, with a strong focus on the Upper-Silesian Coal Basin in Poland, one of the largest regional emitters of methane. The mission utilised a multitude of state-of-the art instruments applied on both airborne and ground based platforms, including active lidar (CHARM-F, see Amediek et al., 2017), passive remote sensing (MAMAP, see Gerilowski et al., 2011; Krings et al., 2013), in situ measurements (CRDS, QCLS; see e.g. Filges et al., 2018), and satellite observations. Wherever possible, these were applied simultaneously in order to a) achieve high observation inter-comparability, b) test the limits of applied measurement techniques, c) provide a rich suite of observations to evaluate atmospheric transport models, and d) to estimate regional GHG emissions.

Here we present the results of in situ observations of atmospheric greenhouse gases and methane isotopic composition obtained over nine research flights of the German research aircraft HALO (High Altitude and LOng Range Research Aircraft) during CoMet 1.0, with the use of two airborne instruments installed aboard the aircraft during the campaign: i) JIG (Jena Instrument for Greenhouse gas measurements), a continuous analyser for measurements of CH_4, CO, CO_2 and H_2O and ii)

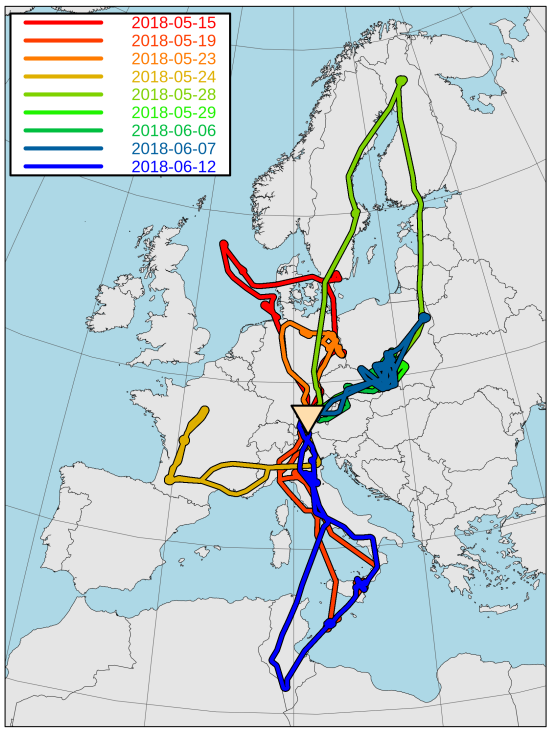

Figure 1. Geographical extent of HALO research flights during the CoMet 1.0 mission.

JAS (Jena Air Sampler), which collected discrete 1 l samples for subsequent laboratory analyses of CH_4, CO_2, H_2, N_2O, SF_6, O_2/N_2, Ar/N_2, $\delta^{13}C-CH_4$ and δ^2H-CH_4.

2 Methods

2.1 CoMet 1.0 flights

During the CoMet 1.0 mission, HALO performed nine research flights, with more than 63 hours of observations over continental Europe and parts of northern Africa (Fig. 1), with the base of operations located in Oberpfaffenhofen (Bavaria, Germany, marked with a triangle in the figure). During the campaign, each flight aimed to reach several scientific goals based on the synoptic meteorological conditions over selected target areas. These goals included, e.g., comparisons between active remote sensing and in situ observations, co-located measurements at satellite overpass points, comparisons against ~~another airborne instrument~~other airborne instruments, and others. For each of those, a specific measurement strategy was adopted. Those relevant for the measurements discussed in this study are described in section 2.3. A complete description of the CoMet 1.0 mission will be given in an overview publication by Fix et al. (in prep, this special issue).

2.2 In situ instrumentation

2.2.1 JIG - Jena Instrument for Greenhouse gas measurements

In situ continuous airborne measurements of greenhouse gases on board HALO have been carried out using JIG (Jena Instrument for Greenhouse gas measurements; photo available in the supplement, Fig. S1). The core of the device is a modified commercial analyser ~~G4201-m~~G2401-m, developed by Picarro Inc. (Santa Clara, CA, USA), which was redesigned in order to fulfil conditions necessary for long-term deployment in the scope of IAGOS ERI (In-service Aircraft for a Global Observing System - European Research Infrastructure). Detailed development of the instrument, with the description of its operational parameters, is described in Chen et al. (2010) and Filges et al. (2015, 2018). Here, only the basic operation principle and main differences to the IAGOS setup are given.

The core method of the measurement is wavelength-scanning Cavity Ring-Down Spectroscopy (CRDS), where an infrared-wavelength laser light is injected into a high finesse optical cavity. In the first phase of the measurement, the strength of the incident laser beam gradually increases over time thanks to the resonance effect in the optical cavity, which also allows for the enhancement of the effective absorption length and thus increases the detector's sensitivity. After reaching the designated signal level, the laser is turned off and the ring-down phase of the measurement begins. The time constant of the resulting exponential decay (ring-down time) depends on the absorption coefficient of the measured compound for the laser wavelength, tuned so that the scan along selected individual spectral lines of the measured molecules is possible. The measurement requires the usage of calibration gases, as well as careful control over cavity pressure and temperatures in order to prevent sample density variations. During the measurements described here, the cavity pressure was set at all times to ~~140.0~~ 186.65 hPa (140 Torr), and the temperature to 45.00 °C, with ~~tollerance levels of~~ tolerance levels of 0.13 hPa (0.1 Torr) and 0.02 °C, respectively.

The instrument reports dry mole fractions, defined as number of molecules of each species in moles per one mole of dry air, with typical observed ranges expressed in $\mu mol\,mol^{-1}$ for CO_2 (equal to one part per million, ppm) and in $nmol\,mol^{-}1$ for CO and CH_4 (equal to 1 part per billion, ppb). As the collected air was not dried in the sampling line, a water correction was applied based on the online measurements of H_2O mole fraction, following the approach described in previous studies of Filges et al. (2015) and Reum et al. (2019).

Calibration of the instrument was performed in the laboratory before and after the CoMet 1.0 mission by measuring three air mixtures, stored in ~~so-called~~ working tanks, which covered the range of ambient ~~mixing ratios~~ mole fractions of CO_2, CH_4 and CO and had assignments traceable to the respective WMO calibration scales. All JIG trace gas ~~mixing ratio~~ mole fraction data provided in the current study are reported on the current WMO calibration scales: CO_2 X2007, CH_4 X2004A, and CO X2014A. The instrument calibration was monitored during the mission with the use of two reference in-flight cylinders ~~containing~~ that contained dry mixtures of atmospheric air of known composition, ~~which~~ for each tracer at a high and a low mole fraction, namely: 373.4 – 397.4 $\mu mol\,mol^{-1}$ for CO_2, 1661.0 – 1917.1 $nmol\,mol^{-1}$ for CH_4, andhttps://sharelatex.gwdg.de/project/5f6d9ab45ba5b4007f24c31c 77.4 – 139.5 $nmol\,mol^{-1}$ for CO. These were analysed several times during each flight. The calibration cycle consisted of two intervals, each ~~five~~ three minutes in length. The ~~initial~~

~~two minutes~~ first minute of each interval ~~were~~ was discarded in subsequent analyses due to pressure equilibration effects within the regulators.

Except for a single calibration check performed prior to take-off during a power-up procedure, all the other calibration check cycles were enabled manually by an on-board operator of the system, during transit phases of the flight, in contrast to the regular IAGOS implementation (Filges et al., 2015, 2018). The in-flight calibration checks occurred at high altitudes, where high gradients of GHGs were not expected and the loss of information could be minimised. The last calibration cycle was always performed immediately before the final approach of the flight. It should be noted that the results of the in-flight calibration checks were only used for assessing a potential drift in the instrument calibration factors relative to the pre-mission (April 2018) and post-mission (November 2018) laboratory calibrations.

Additional, independent verification of the measurement quality was carried out by comparison of the ~~mixing ratios~~ mole fractions from in situ measurements and those obtained from laboratory analyses of air samples collected by the JAS (Jena Air Sampler, see sec. 2.2.2, and the discussion of the results in section 3.1).

Two malfunctions of the JIG occurred during the CoMet 1.0 mission. On May 28th (flight no. 5), a software issue (i.e. clock reset) caused the loss of 96.8 % of in situ data from that day. The remaining 3.2 % have been excluded from the following analysis due to their fragmentation. The second malfunction occurred during the power-up procedure on June 7th, 2018 (flight no. 8), when JIG suffered an unexpected shutdown due to cabin overheating, which required a manual reset of a temperature switch. This in turn caused unintentional damage to the optical fibre mount located inside the instrument housing. The resulting loss of signal strength caused deterioration of the system parameters over flights no. 8 and 9, increasing noise and shifting the instrument calibration parameters. These were subsequently corrected using in-flight calibrations and post-mission laboratory calibrations. The impact of the malfunction and final effect of applied corrections is discussed in section 3.1.

2.2.2 JAS - Jena Air Sampler

The sampler used during CoMet 1.0 (Fig. S1) is an airborne version of the automated flask sampler developed within the ICOS (Integrated Carbon Observing System) infrastructure. The device is equipped with 12 slots for holding one litre glass flasks with automatically operated valves at both ends. Sample air, collected outside the aircraft fuselage with a dedicated inlet, flows through tubing (PFA, 415 cm, 6.35 mm (1/4 in) OD) and into the drying unit (70 cm^3, ~~SS~~stainless steel) filled with magnesium perchlorate. The dryer is connected via another tubing section (PFA, 317 cm, 6.35 mm (1/4 in) OD, plus additional 15 cm of 6.35 mm (1/4 ~~OD, SS~~in) OD, stainless steel, for pressure sensor mount) to a Teflon diaphragm pump (N 813.3, KNF Neuberger GmbH) that provides the over-pressure necessary to flush and pressurise the flasks, up to approximately 1500 hPa. The pump is connected directly to the main input manifold (passing through all three rack-mounted sub-units) via another flexible tube (PFA, 156 cm, 6.35 mm (1/4 in) OD). The input manifold can be connected to the output line either via open flasks (one or more), or a two-way bypass valve. Each flask has its own pair of automated motors responsible for operating its input (upstream) and output (downstream) valves. At the end of the sampler flow line, a mass flow meter (MFM~~) (~~; model D6F-20A6-000, Omron) is installed that integrates the total volume of air flowing through an opened flask, which ensures that the flask volume has been sufficiently flushed with the sampled air (at least 6 l under normal conditions). At the outlet of the

system, a pressure release valve is installed that maintains the pressure at 1.5 bar, and prevents the back-flow of the pressurised cabin air into the sampler in case of power failure. Three pressure sensors and three thermometers are also installed to monitor the status of the system.

The sampler ~~is~~ was controlled via computer in the electronic control section using dedicated software. The procedure for flask flushing and filling ~~is~~ was enabled manually by an operator, either at pre-determined flight altitudes (in the case of measurements of vertical profiles) or locations (e.g. plume sampling). Each flask was flushed with 10 times its volume prior to closing the upstream and downstream valves. Typically, flasks were filled during descending profiles, but on some occasions also during ascents. The variable ambient pressure caused the flask fill time to vary between 100 seconds at high altitudes to 25 seconds close to the surface.

In order to precisely establish spatio-temporal coordinates from which the sample is collected, a flow model has been used that takes into account i) flow information from the MFM, ii) the volume of tubing elements such as the dryer and tubing, and iii) the varying physical length of tubing between the inlet and the flask inlet slots (ranging from 10.76 m to 15.58 m). For each collected sample, a temporal weighting function was calculated that represents the collected air volume, following the approach suggested by Chen et al. (2012).

All flasks collected aboard HALO during CoMet 1.0 were analysed in the GasLab of the Max Planck Institute for Biogeochemistry (MPI-BGC) in Jena, Germany, to establish ~~mixing ratios~~ mole fractions of trace gases (CO_2, CH_4, N_2O, H_2, SF_6) based on their respective WMO scales. Gas chromatographic analysis of air in glass flasks is made with a gas chromatographic system based on two GCs (6890A, Agilent Technologies) equipped with a flame ionisation detector and a Nickel CO_2 converter (FID) for CH_4 and CO_2, an electron capture detector (ECD) for N_2O and SF_6, a helium ionisation pulsed discharge detector (D-3-I-HP, Valco Instruments Co. Inc.) for H_2, and a HgO Reduction Gas Analyser (RGA3, Trace Analytical) for H_2 and CO. Additional analyses of O_2/N_2, Ar/N_2 and isotopic composition of methane ($\delta^{13}C-CH_4$ and $\delta^{2}H-CH_4$) were carried out in the IsoLab of MPI-BGC (Sperlich et al., 2016). The typical measurement precision of the laboratory analyses is given in Table 1.

A significant ~~drift in mixing ratios was observed over the~~ (approximately 10 $\mathrm{nmol\,mol^{-1}}$) bias in CO mole fractions was observed when comparing in situ measurements from JIG against gas flasks collected using JAS. Control laboratory experiments run after the campaign have shown that this bias was a result of a growth in CO mole fractions in the period between sample collection and ~~the subsequent measurement in the GasLab. The resulting~~ subsequent laboratory analysis. This enhancement in the ~~mixing ratio was not easily correctable, therefore the results had to be discarded~~mole fraction could be attributed to new valve sealing polymer but could not be accurately corrected, therefore we have decided to discard these results. Careful quality control and additional tests did not show any ~~signs~~ sign of other gases being affected.

2.3 Flight patterns

Depending on the scientific goals set out before each research flight, different flight patterns were executed in order to obtain the most valuable data. The main strategies adopted for the CoMet 1.0 mission were: i) long-range gradient observations, designed to maximise the amount of observations for active lidar measurements with CHARM-F operated on HALO, ii) vertical profiles,

Compound	Precision	Uncertainty of scale link	Unit
CO_2[a]	0.065	0.046	$\mu mol\ mol^{-1}$
CH_4[a]	1.3	0.70	$nmol\ mol^{-1}$
N_2O[a]	0.13	0.12	$nmol\ mol^{-1}$
H_2[a]	0.31	0.28	$nmol\ mol^{-1}$
SF_6[a]	0.044	0.025	$pmol\ mol^{-1}$
O_2/N_2[b]	1.5	1.6	per meg
Ar/N_2[b]	4.5	6.0	per meg
$\delta^{13}C-CH_4$[c]	0.046	0.12	‰
$\delta^{2}H-CH_4$[c]	0.49	1.4	‰

[a] - Precision calculated as the standard error of the repeated flask measurements (usually between three to five). An average standard error for complete set of flasks collected during CoMet 1.0 is given. Uncertainty of the scale link specified as root from sum of squared uncertainties of: i) specified CCL (Central Calibration Laboratory) scale transfer uncertainties, ii) precision limit of individual laboratory standard calibration events, and iii) response drifts between successive calibration events. For H_2, scale transfer uncertainty is equal to zero by definition, as flasks were measured directly against the primary scale. This uncertainty estimate does not include the accuracy of the respective WMO scale.
[b] - O_2/N_2 and Ar/N_2 measurements were done on the BGC-IsoLab local realisation of the Scripps scale. Realisation is achieved through the regular measurements of in-house standards against independently calibrated tanks from Scripps. Reproducibility estimate is given as the average of standard deviations calculated from measurements against in-house standards (IsoLab, MPI-BGC, Jena) of three cylinders with air mixtures calibrated independently at Scripps Institute for Oceanography (SIO), covering the O_2/N_2 range between -262.2 per meg to -807.6 per meg and Ar/N_2 range of 136.5 per meg to 167.1 per meg.
[c] - Only a single measurement of each sample was possible. Precision estimated using repeated working standard measurements performed in sequence with the sample (usually four or five per sample). Reproducibility defined according to Sperlich et al. (2016).

Table 1. Average measurement uncertainties of the flasks collected during CoMet 1.0. All values given with with coverage probability of 0.68. A correction factor based on a Student's t-distribution was applied to account for low population size, following the Guide to the Expression of Uncertainty in Measurement (JCGM, 2008).

aimed mainly at the intercomparison between the lidar and in situ observations and iii) low-altitude legs, performed to assess the enhancements of CO_2 and CH_4 downwind of their sources (plume-chasing).

2.3.1 Large-scale variability in upper troposphere and lower stratosphere

Due to the constraints related to using other instruments (the active lidar), a significant amount of flight time was spent flying level at altitudes higher than 4 km, in order to emulate a flight path similar to that of a satellite system. Typical variability of in situ greenhouse gas ~~mixing ratios~~ mole fraction was low in these cases and is usually considered to be caused by intermixing of air masses coming from different regional source areas. In situ data obtained in this manner are well-suited for validation

of Global Chemistry Models. As an example, in sec. 3.2 we compared JIG observations against well established modelling products: CAMS greenhouse gas forecasts. A detailed model description is given in sec. 2.4.

2.3.2 Vertical profiles

Multiple vertical profiles of the atmosphere were carried out during the campaign in order to establish the connection between column-integrated remote sensing and in situ measurements, thus also linking remote sensing observations to common WMO scales for greenhouse gases. The typical strategy consisted of i) a high-altitude overflight over a selected target, ii) descent in the form of a spiral to the lowest possible altitude above the target, iii) subsequent ascent back to high altitude, usually flown along the shortest path in the direction of the next planned way-point.

Usually two or three vertical profiles were executed during a given flight, depending on the availability of points of interest and airspace accessibility. Wherever possible, profiles were executed above a) ICOS stations, b) TCCON stations (Total Carbon Column Observing Network), c) Sentinel 5P or GOSAT overpass locations. Flasks were also collected during vertical soundings, at levels distributed between the minimum and maximum altitude, typically consisting of six samples per profile (in some cases reduced to four).

Measurements of vertical profiles are also of high interest for model validation exercises, as the availability of highly precise data on greenhouse gases over Europe is currently still limited. In the scope of the current study, we have assessed the performance of two well-established modelling products (CAMS and Jena CarboScope, see sec. 2.4) against CoMet 1.0 in situ observations.

2.3.3 Measurements in the planetary ~~bounary~~ boundary layer - plume chasing and isotopic composition

A limited amount of data were also collected inside the planetary boundary layer (PBL), usually during the lowest stage of vertical profile sounding. In several cases, however, these PBL sections were extended in order to cross low-level emission plumes (plume chasing). Of particular interest here are the flights over the Upper Silesian Coal Basin (a large regional methane source) and downwind of the Bełchatów coal power plant (the largest single emitter of CO_2 in Europe, according to the European Pollutant Release and Transfer Register, v16; E-PRTR, 2019). For both of these sources, clear enhancements from the strong sources were captured when crossing the plume downwind.

Additional to the in situ measurements, flasks were also collected to gather information about additional compounds and the stable isotopic composition of CH_4. For the cases where sufficient data were available, we have applied the method of Miller and Tans (2003), a variation of a classic Keeling model (Keeling, 1958), in order to obtain the isotopic mean source signature (δ_0), expressed using relative delta notation. The method assumes a two-factor mixing of background air and methane-enhanced plume:

$$\delta_{obs}\chi_{obs} = \delta_0\chi_{obs} - \chi_{bg}(\delta_{bg} - \delta_0), \tag{1}$$

where δ_{obs} is the measured isotopic signature, δ_{bg} is the background signature, χ_{obs} is the ~~mixing ratio~~ mole fraction of the analysed compound, and χ_{bg} is the background ~~mixing ratio~~mole fraction. Here, similar to the Keeling approach, information

on δ_0 can be gleaned from the application of linear regression, however the source signature is calculated from the slope, rather than intercept, of the linear fit formula. Following the study by Cantrell (2008), we have applied a Williamson-York regression, which allows one to take into account uncorrelated errors in both the X- and Y-axes of the data.

The Miller-Tans method relies on the appropriate assignment of the background signature (i.e. of the atmospheric air outside of the plume). Long term data available from atmospheric observations show that the isotopic composition of methane in the atmosphere is variable (Röckmann et al., 2016; Nisbet et al., 2019) in both space and time. In order to estimate the background signature, ~~here~~ we have used measurements from air samples collected in the immediate vicinity of the target plume, either from ~~i)~~ the upwind air masses ~~when possible or ii) air~~ or from outside of the main plume~~when not~~.

2.4 Models

As part of the Copernicus Atmosphere Monitoring Service (CAMS), the European Centre for Medium-Range Weather Forecasts (ECMWF) performs greenhouse gas simulations based on its Integrated Forecasting System (IFS) and provides operational global forecasting products focused on greenhouse gases. In this work, we have used the five-day high resolution greenhouse gas forecast product from CAMS (experiment ID: gqpe, downloaded in April 2020; see Agusti-Panareda et al., 2017; Agustí-Panareda et al., 2019) in order to validate the model using our observations. Further in the text, we will refer to these data as CAMS for simplicity. Satellite data were used for initialization of the forecast, namely TANSO-GOSAT for CO_2 and CH_4 and additionally MetOp-IASI for CH_4 (Massart et al., 2014, 2016). For CO, CAMS operational analysis (Inness et al., 2015, 2019) was used for forecast initialization. Original CAMS 1-day forecast data, available at TCo1279 Gaussian cubic octahedral grid (equivalent to approximately 9-km horizontal resolution) was interpolated to 0.125° x 0.125°. The frequency of the analysed CAMS data was 3-hourly, and vertical resolution was the regular L137 ECMWF configuration.

Additionally, CO_2 data were also compared to the Jena CarboScope product (version s04oc_v4.3, Rödenbeck, 2005), further referred to as CarboScope. While the resolution of the driving CarboScope model output fields is much lower in this case (4° x 5° horizontal), the system benefits from using the fluxes of CO_2 optimized using a Bayesian inversion framework. A detailed description of the modelling system is given in Rödenbeck et al. (2003) and Rödenbeck (2005). The transport model TM3, which is used by CarboScope, is described in Heimann and Körner (2003).

3 Results & Discussion

3.1 Overview and data quality

A total of 55 hours and 17 minutes of high-frequency (1 Hz) observations of CO_2, CH_4 and CO were obtained aboard HALO in the scope of the CoMet 1.0 campaign. Measurements of CO_2 are presented in Fig. 2, and a full overview, including also CH_4 and CO is available in the supplement (Fig. S2). Observations were performed at altitudes ranging from approximately 50 m up to 14 km above mean sea level. Data from 51 vertical profiles are available~~these are listed in the supplement, Table S1),~~ , out of which 21 have simultaneous flask measurements. They are listed in the supplement (Table S1). 15 in-flight calibrations were

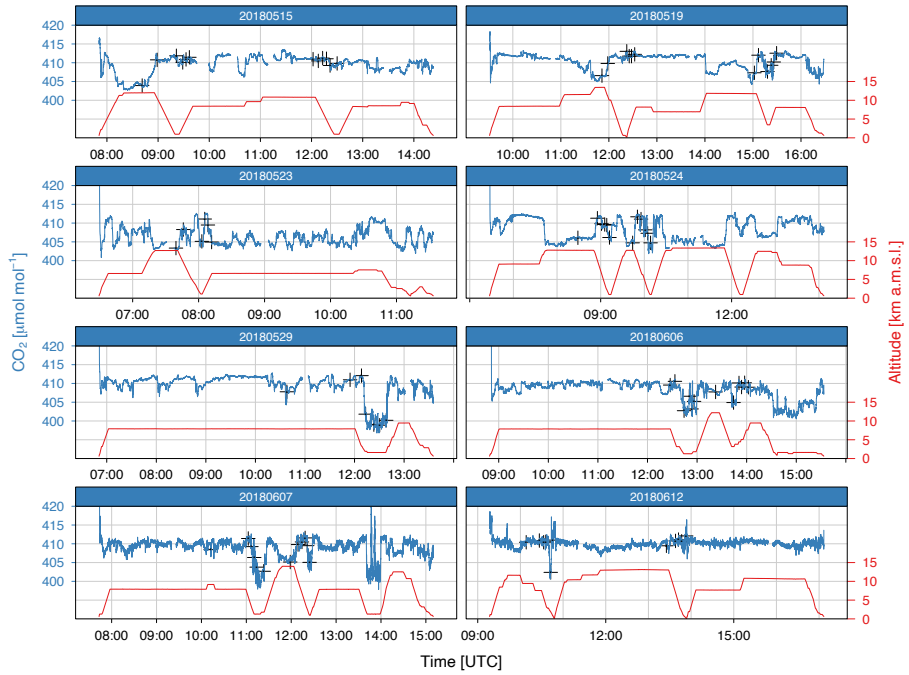

Figure 2. In situ ~~mixing ratios~~ mole fractions of CO_2 measured throughout CoMet 1.0 with flight altitudes. Shading corresponds to the vertical profiles discussed throughout the manuscript. Shading colours denote: blue – ascending profile, red – descending profile. Co-located flask measurements are marked with black crosses.

performed, making it possible for the single-measurement precision to be estimated for flights no. 1–7. These were equal to: 0.06 µmol mol^{-1} (CO_2), 0.3 nmol mol^{-1} (CH_4) and 3.1 nmol mol^{-1} (CO) . Malfunction during the roll-out procedure prior to flight no. 8 caused deterioration in the instrument noise for two subsequent flights (no. 8 and 9), with values of precision increasing to 0.3 µmol mol^{-1}, 1.5 nmol mol^{-1} and 50 nmol mol^{-1} for CO_2, CH_4 and CO, respectively.

Results from in-flight measurements of the two reference cylinders showed no significant drift, however the flight-to-flight variation of each low- and high-span measurement during the period prior to the instrument malfunction on June 7th was slightly larger than expected for CO_2: low-span measurements varied by 0.10 µmol mol^{-1}, 0.4 nmol mol^{-1}, and 1.0 nmol mol^{-1}, while high span measurements varied by 0.14 µmol mol^{-1}, 0.3 nmol mol^{-1}, and 0.8 nmol mol^{-1} for CO_2, CH_4 and CO, respectively. The likely cause for this are the silicon rubber membranes used in the pressure regulators (Filges et al., 2015), which are known to cause diffusion of CO_2 (Hughes and Jiang, 1995). Given that species other than CO_2 did not show unexpected behaviour, we did not apply any correction of the measurements resulting from the in-flight measurements of the reference cylinders. For this reason, we also did not apply any correction of drift within each flight, in contrast to the experience of Karion et al. (2013b).

The comparison between flask and in situ measurements is available for all except one flight (no. 5). From the ~~total~~ 96 samples collected and analysed, 84 had simultaneous in situ measurements available from JIG that could be used for a bias

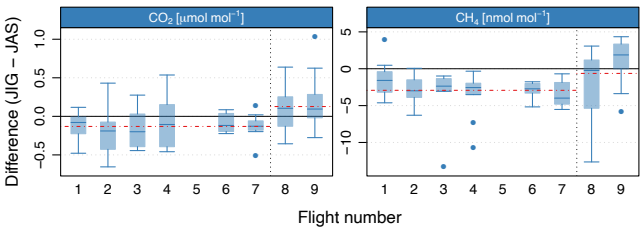

Figure 3. Comparison between JIG results and analysis of flasks collected during CoMet 1.0 aboard HALO. Data from the last two flights (separated by the dashed line) indicate a residual change in calibration, following an instrument malfunction. See text for details.

assessment. Here, we compare bias between both our datasets to 'network compatibility goal', defined by World Meteorological Organization as "the scientifically-determined maximum bias among monitoring programmes that can be included without significantly influencing fluxes inferred from observations with models" (WMO, 2019). WMO specifies this compatibility goal as equal to 0.1 µmol mol^{-1} for CO_2 (in the northern hemisphere) and 2 nmol mol^{-1} for both CH_4 and CO.

As shown in Fig. 3, the average bias for flights 1–7 was equal to -0.131 (30) µmol mol^{-1} for CO_2 and -2.93 (32) nmol mol^{-1} for CH_4, where ~~number in brackets~~ numbers in parentheses represent standard uncertainty in the final digits quoted for the numerical value. Larger spread when independent measurements are considered (Fig. 2) stems mainly from the imperfect match between the temporal coordinates of the two instruments, which can be considered random and does not cause systematical shift. After the malfunction (see section 2.2.1), i.e. for flights no. 8 and 9, these mean offsets were equal to 0.127 (68) µmol mol^{-1} and -0.64 (91) nmol mol^{-1} for the respective gases. While the difference of values ~~caused by the broken mounting~~ as compared to flights 1–7 is statistically significant, ~~the difference~~ it is still close to the WMO compatibility goal.

3.2 Large Scale Variability

Out of the total amount of observations during CoMet 1.0, 84 % were performed at altitudes above 4 km and are of particular interest for model validation. To demonstrate the utility of the observations to validate model results, as well as to help understand the patterns in measured ~~mixing ratios~~mole fractions, we analyse and compare JIG measurements to CAMS high-resolution products for CO_2, CH_4 and CO. Flight no. 2 ~~,~~(shown in light red in Fig. 1~~,~~) is discussed as an example.

The flight (Fig. 4, top) was executed on May 19th 2018, with the main goal of capturing large-scale variability of greenhouse gases in the atmosphere above Italy and the Mediterranean coast. Two vertical profiles were planned above ICOS stations, namely Lampedusa (35° 31′ 05" N, 12° 37′ 50" E) and the Monte Cimone mountain station (Tuscan-Emilian Apennines, 44° 11′ 38" N, 10° 42′ 05" E). The latter profile was executed approximately 20 km away from the target due to an active thunderstorm over the site. Other points of interest were i) the Po valley, crossed twice (morning and afternoon) at high altitude and ii) two high-altitude circles around Mount Etna (35° 31′ 05" N, 12° 37′ 50" E).

Fig. 4, bottom, shows the CAMS model results extracted at the geographical aircraft time and location, together with corresponding in situ observations from JIG overlaid on the aircraft flight path, both plotted using the same colour scale. The

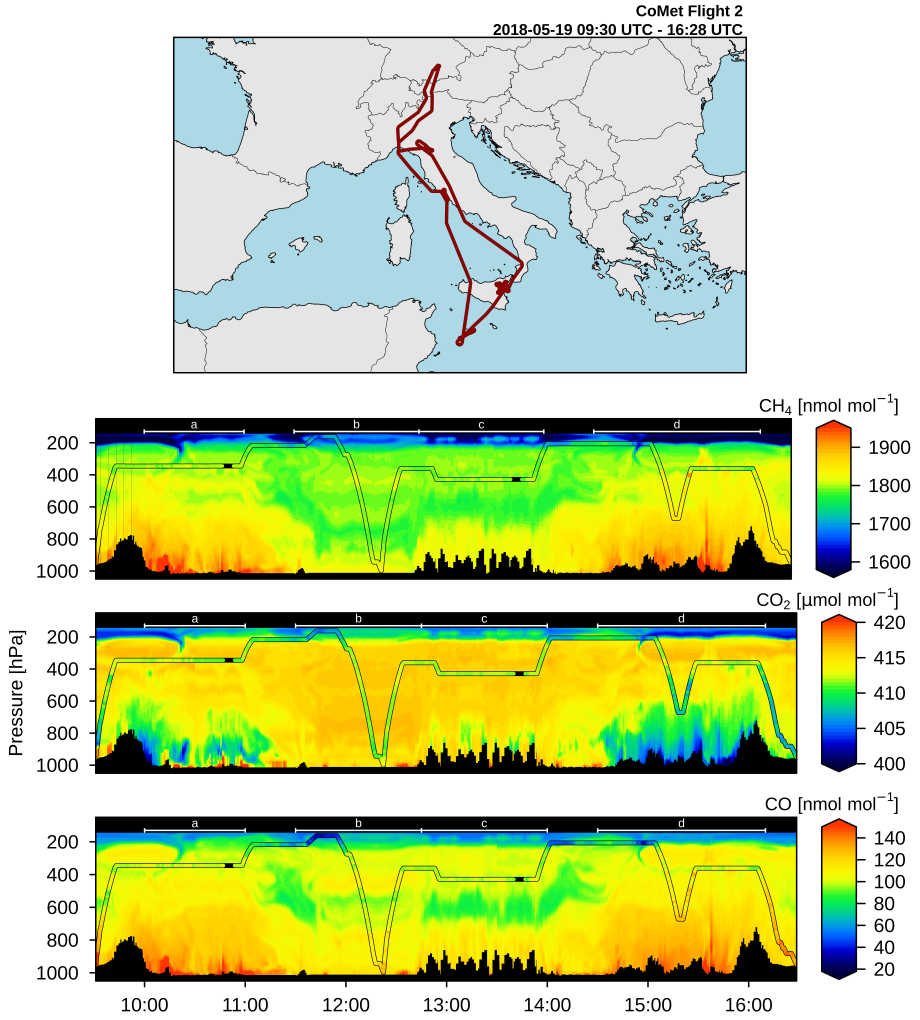

Figure 4. Curtain plot showing results for May 19th, 2018. Top~~row~~: Overview map with flight path~~(left), and map zoomed over flight area (right); other~~ . Other rows: time series of aircraft altitude, with CAMS model results as colour plot in background for CH_4, CO_2, and CO (top to bottom); coloured lines superimposed on the curtain plot denote in situ measurements from HALO, with ~~mixing ratios~~ mole fractions plotted in the same colour scale. Ranges a–d denote distinct sections of the flight, namely: a) initial southward crossing of the Po valley, b) passage over Mediterranean towards Lampedusa ending with a vertical sounding near the ICOS station, c) circular flights over Mt. Etna, d) northward flight over northern Italy with a profile attempted over Mt. Cimone. See the discussion in the text for details.

model captures most of the features observed in the atmosphere. Speaking in terms of observed spatial and temporal variability of the atmospheric composition (modeled and observed), four sections of the flight can be identified: a) morning overflight over northern Italy, b) passage over Mediterranean Sea, ending with a vertical sounding at Lampedusa, c) circling Mount Etna

at medium altitude and d) northward flight over Italy, including a vertical profile in the vicinity of Monte Cimone, with a subsequent crossing of Po Valley and the Alps, ending with landing at home base.

During the first section of the flight (Fig. 4, a), after the initial climb, the aircraft stayed at high altitude (300 hPa, ~~approx.~~ approximately 8 km a.m.s.l.), sounding the free troposphere above the Po Valley. Comparison of measured concentrations to the model suggests that the chosen flight level was well within the free troposphere. Close to the surface, CAMS predicted high enhancements of greenhouse gases, clearly visible on the CH_4 and CO plots. At the time (10:00–11:00 UTC), the boundary layer was still developing, reaching only about 900 hPa level (approximately 1000 m).

After crossing the coastline, the aircraft ascended to a cruise altitude of ~~approx.~~ 250 hPa (approximately 12 km). Around 11:30 UTC it reached the tropopause level, and, after another increase in altitude, entered into the stratosphere for ~~approx.~~ approximately 10 minutes immediately prior to the vertical sounding at Lampedusa ~~.~~ (Fig. 4, b). The vertical structure of the atmosphere was generally well predicted in the model (see sec. 3.4, and also Fig. S3-S18 in the supplement), albeit larger differences can be observed in the lowest 3 km of the profile, especially for CO_2.

The Mt. Etna section of the flight (Fig. 4, c) took place mostly in the free troposphere and no significant gradients were observed for either of the measured compounds. Subsequent transfer over southern Italy (~~section~~ d) started with an ascent into the stratosphere (at ~~approx.~~ approximately 220 hPa, 13 km a.m.s.l.). After ~~approx.~~ 10 minutes of northward flight, the aircraft crossed into the troposphere horizontally again.

Immediately before the descent to Monte Cimone it crossed a stratospheric ~~intrusion, possibly caused by the intensive deep convective mixing occurring~~ air filament, possibly brought down to the flight level by the outflow of a deep convective system active in the area in the afternoon on that day. ~~After~~ This is corroborated by CAMS model results, which show a clearly defined air-mass structure, depleted in mole fractions for all the observed compounds, stretching from the stratosphere at 200 hPa down to approximately 400 hPa (corresponding to roughly 13 km and 8 km a.m.s.l., respectively). Shortly after that the aircraft descended, making a downward spiral over the northern Apennines, down to ~~approx.~~ approximately 700 hPa (3.5 km). The model-observation discrepancy is much higher at this point, most probably due to: i) errors in representation of the local convective systems, or ii) errors in the surface fluxes driving the modelled ~~mixing ratios~~mole fractions, or the mixture of both. The high resolution CAMS product correctly captures most of the large scale phenomena. There are, however, specific situations where the performance of the model drops, specifically in the vicinity of strong local convection systems, where parameterisations can sufficiently predict neither the height nor the transport of the strong enhancements present in the Po valley. The reasons behind this discrepancy may stem from the inability of coarser scale parameterisations to capture local phenomena accurately, or from an incorrect distribution of the ground-level sources.

In the following section, we analyse the model-data mismatch more closely using the subset of CoMet 1.0 data collected only during the vertical soundings.

3.3 Vertical structure of the atmosphere

All profiles of CO_2, CH_4 and CO collected with JIG are presented in Fig. 5, together with comparison to the CarboScope and CAMS model products. Individual comparisons are available in the supplement (Fig. S3-S10 and S11-S18). It should be noted

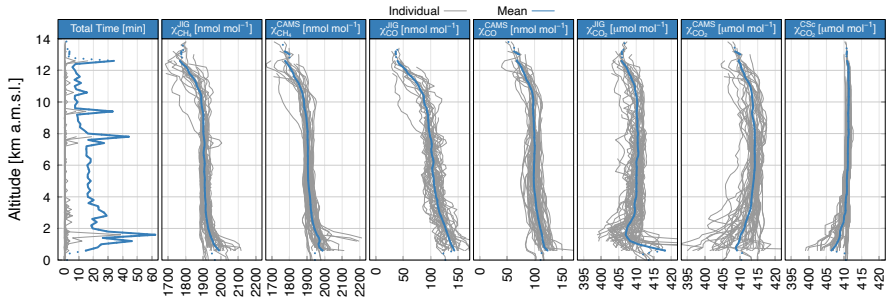

Figure 5. An overview of the vertical profiles measured during the CoMet 1.0 mission, together with modelled profiles from CAMS and CarboScope (denoted with ~~TM3~~CSc). In the first panel, total time is calculated as a sum of 1-s observations from each respective bin. All the other panels present ~~mixing ratios~~ mole fractions for different variables, binned into 200 m layers. Averages for each layer are shown as a solid blue line while solid grey lines represent individual profiles. Dashed lines represent the means with less than 200 seconds of observations available. Only data from the individual profiles marked on Fig. 2 are plotted here, i.e. the measurements collected during horizontal sections of the flights are not included.

that the mean profile for the lowest altitudes is dominated by a limited amount of cases when the ground level was reached. This happened most often at home base (EDMO, Oberpfaffenhofen). Similarly, only a limited number of profiles reached altitudes beyond 12 km above mean sea level.

Again, three distinct altitude ranges can be distinguished based on the observed gas ~~mixing ratios~~ mole fractions and their variance. The lowest, the PBL, is characterised by highly variable concentrations and is located in the altitude range of 0–3 km. Both the highest and lowest observed concentrations of CO_2 were observed here, with most of the observations in the range between 400 and 420 $\mu mol\,mol^{-1}$. Occasionally, peaks of over 420 $\mu mol\,mol^{-1}$ were observed in the vicinity of strong point sources (e.g. Bełchatów power plant). CH_4 and CO variability was also high, with most observed values between approximately 1880 and 2000 $nmol\,mol^{-1}$ for methane (with peaks above 2100 $nmol\,mol^{-1}$) and 100–150 $nmol\,mol^{-1}$ for carbon monoxide.

Above the PBL range, free tropospheric observations were characterised by much smaller variability. For CO_2 the mean profile becomes flat with a value of 410 $\mu mol\,mol^{-1}$ up to approximately 10 km altitude. For CH_4 and CO a vertical gradient in the mean values is observed, reflecting the balance between surface anthropogenic sources, large-scale advection and tropospheric chemical sinks.

Above the altitude of 10 km, a more pronounced decrease in the ~~mixing ratios~~ mole fractions is observed, which is directly related to occasional crossings into the tropopause region and the lowermost stratosphere. The variability of the observed decrease is large and follows the variability in the tropopause height. On average we have observed a 4 $\mu mol\,mol^{-1}$ decrease for CO_2 between 10 km and 13 km, which is most probably caused the increasing age of the slow-mixing stratospheric air (Andrews et al., 2001). Decreases of CH_4 and CO are more pronounced (on average 150 $nmol\,mol^{-1}$ and 70 $nmol\,mol^{-1}$, i.e. 8 % and 45 % relative to the value at 10 km), underlining an increased oxidative breakdown of these tracers (added to the age effect in case of CH_4).

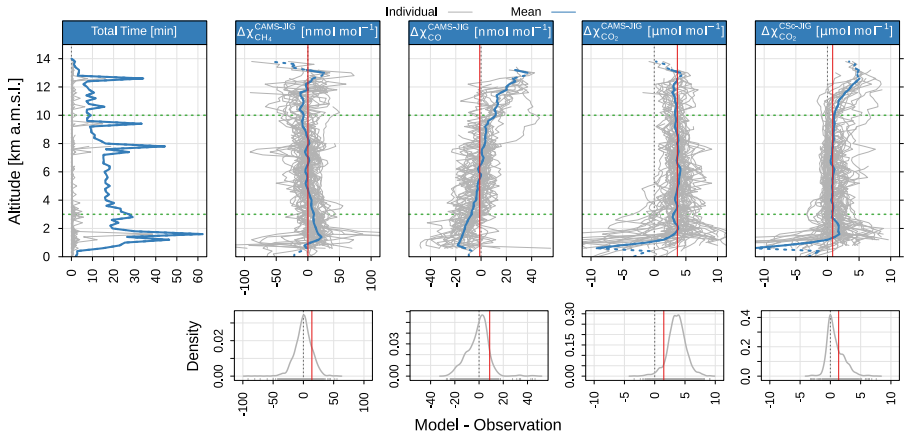

Figure 6. Top row: The first panel shows time spent in each altitude bin (~~200m~~200 m) for individual flights (grey lines) and the sum for CoMet 1.0 (solid blue). The four panels to the right show differences between modelled (CAMS and CarboScope, ~~here marked~~ latter abbreviated as ~~TM3~~CSc) and measured ~~mixing ratios~~ mole fractions as a function of altitude (grey - individual flights, blue - average per altitude bin). Dashed red line represents the average value between the altitude range 3–10 km (vertical range marked with horizontal dashed green lines). Bottom: density plots for measurements in the free-tropospheric (3–10 km) range.

While the observed gradient is similar to previously reported studies (e.g. Wofsy, 2011; Sweeney et al., 2015; Umezawa et al., 2018), measurements from CoMet 1.0 also clearly indicate the increase in atmospheric concentrations over the past years. For example, the CH_4 ~~mixing ratios~~ mole fractions measured during the IMECC campaign in autumn 2009 (Geibel et al., 2012) were approximately 60 $\mathrm{nmol\,mol^{-1}}$ lower throughout the atmospheric column than those observed in 2018. This number is closely in line with mean global atmospheric growth of methane of 63.8 $\mathrm{nmol\,mol^{-1}}$ (between 2009 and 2018 NOAA, 2020).

3.4 Model validation

The vertical profile subset of the measurements was the basis of the comparison to the well-established global modelling systems CAMS and CarboScope. Here, we focus on describing the vertical structure of the model-data mismatch, defined as the difference between the modelled results and in situ observations from JIG, presented in Fig. 6. Mirroring previous discussion of different characteristics of the atmosphere, here the different nature of discrepancies can also be separated into three distinct layers of the atmosphere. It is worth noting that the model-observation mismatch is, in general, constant in neither space nor time, as can be seen when analysing the variability between different flight days. However, some important conclusions can be drawn when analysing the overall vertical structure in the difference between global model results and CoMet 1.0 in situ observations.

The variability in the mismatch is highest closest to the surface (bottom 3 km), which is related to influences from local sources/sinks, as well as variability of atmospheric mixing and transport in the PBL, which are hard to represent at respective

model resolutions (0.125° x 0.125° for CAMS, 4° x 5° for CarboScope). Another source of mismatch is related to uncertainties in the emissions data used by the models. Validation of individual emission sources, while of critical importance, remains challenging. In addition, in the case of biospheric CO_2, the prediction of fluxes on scales relevant for direct comparison of ~~mixing ratios~~ mole fractions on regional scales also remains a difficult task. This is true for all the analysed compounds and both models, with a markedly larger discrepancy in the CarboScope product that clearly suffers as a result of its low spatial resolution. As the in situ measurements from CoMet 1.0 are not numerous enough to give a robust estimate for the European region, and differences between the model predictions and observations will be heavily dependent on a specific synoptic range and distribution of sources in the vicinity, we do not provide any general statistics for this lowest part of the atmosphere.

In the free-tropospheric range, the mismatch represents large-scale offset between the model and observations better, and is only weakly dependent on the spatial distribution of the emissions sources. Under this assumption, the mismatch is mostly caused either by i) large (i.e. at least national) scale offsets in emission strengths, ii) bias in the initialisation of the forecasted fields (with CAMS GHG and operational analysis fields which are a combination of model simulation and satellite observations), iii) errors in chemistry parameterisations (OH radical reaction chains, CH_4 and CO).

In the CAMS product, the offset between the modelled values and observations in the troposphere becomes stable with height for CH_4 and CO_2, with a symmetric distribution around a mean value (CH_4: 0 (14) $\mathrm{nmol\,mol^{-1}}$; CO_2: 3.7 (1.5) $\mathrm{\mu mol\,mol^{-1}}$, where standard uncertainty in the final digits is given in brackets. For CO_2, a substantial offset is still present, most probably connected with errors in the strength of the net biospheric fluxes predicted in the model. This general offset needs to be taken into account if the data are either compared directly to the measurements (this manuscript) or used as lateral boundary conditions for regional modelling studies. For CO, a sloped model-data mismatch is observed, most likely related to known issues with the inventories of anthropogenic emissions of CO (e.g. Boschetti et al., 2015) superimposed on chemistry-related effects. The mean value of the offset of CO in the 3–10 km altitude range is equal to -1.0 (8.8) $\mathrm{nmol\,mol^{-1}}$.

For altitudes above 10 km, the mismatch between CAMS and observations shows larger variability for CH_4 and CO, with CO_2 discrepancies similar to those observed in the free troposphere. While the number of observations at these higher altitudes is relatively low compared to those below 10 km, we believe that these differences are also caused by errors in both transport and chemistry schemes in the IFS system. These have been investigated in some detail in the case of CH_4, for which the errors in the stratosphere have been found to be larger than those observed in the troposphere (Verma et al., 2017).

Optimised CO_2 ~~mixing ratios~~ mole fractions from CarboScope also show overall good agreement when compared to observations, despite lower model resolution compared to CAMS. The model-data mismatch is dominated by a random term in the free tropospheric range (0.8 (1.3) $\mathrm{\mu mol\,mol^{-1}}$). Interestingly, the distribution of the mismatch in this altitude range is a positively skewed Gaussian curve (Fig. 6, bottom-right panel), with the values in the main peak almost symmetric around 0 $\mathrm{\mu mol\,mol^{-1}}$, and the ~~tail being responsible for most of the~~ mean offset in the ~~3–10~~ 3 – 10 km range driven by the values in the tail of the distribution. The most probable cause is the inability of the model to represent convective uplifting of CO_2-depleted air from the PBL. It should also be noted that in the CarboScope product, a systematic over-prediction of CO_2 ~~mixing ratios~~ mole fractions above 10 km (up to 5 $\mathrm{\mu mol\,mol^{-1}}$) is observed, which might be caused either by i) significant errors in the tropopause height or ii) too fast vertical mixing in the lower stratosphere, leading to underestimation of the gradient and the

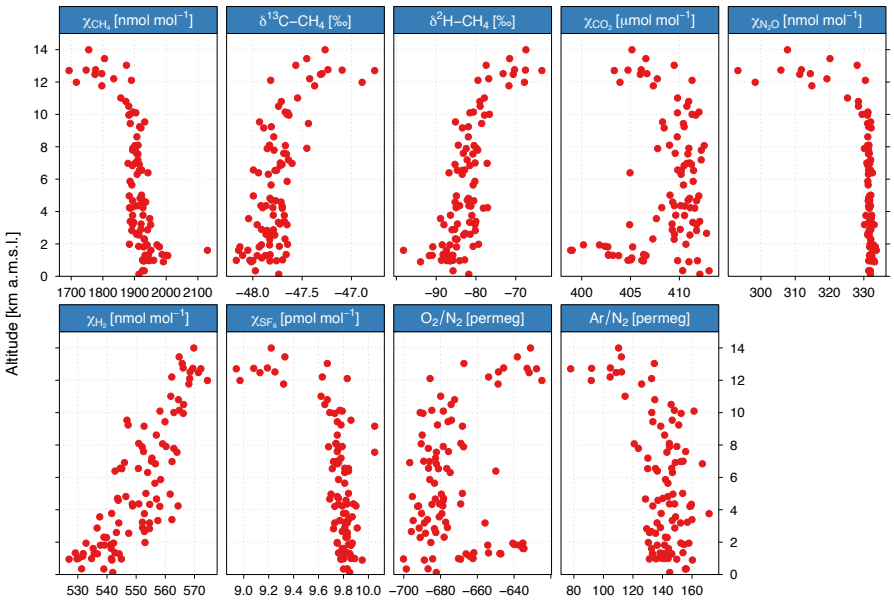

Figure 7. Combined results of air composition ~~from~~ as measured in flask samples collected during CoMet 1.0 aboard HALO.

chemical age of CO_2. In the PBL range, the ~~mixing ratios~~ mole fractions are generally underestimated, sometimes by more than 10 $\mu mol\,mol^{-1}$, albeit such a large discrepancy is only visible for the lowest altitude range (less than 1 km), where the sample size is low. Where the observation set is more robust, the bulk of observations is characterised by ~~discrepancies~~ differences smaller than 10 $\mu mol\,mol^{-1}$ and can have either positive or negative sign. Such behaviour is to be expected when trying to compare local plume enhancements to the low-resolution model results that averages over large, inhomogeneous areas characterised by a dynamic spatio-temporal diurnal cycle of fluxes.

3.5 Additional data from discrete samples - JAS

Figure 7 presents additional data acquired throughout the campaign with discrete samples, with a detailed overview provided in the supplement (Fig. S19 and Table S1). Apart from CH_4 and CO_2, for which the flask data were used for validation, important constituents were monitored, offering further insights into the state of the atmosphere over Europe during the CoMet 1.0 mission. The general nature of the collected data follows the patterns described for in situ data, with three distinct abundance regimes: i) PBL, ii) residual layer / free troposphere and iii) tropopause and lower stratosphere, however with some marked differences.

For N_2O and SF_6, both potent greenhouse gases (IPCC et al., 2013), there is no clearly visible ~~mixing ratio~~ mole fraction gradient between the PBL and the free troposphere. For both gases, the variability is known to be dominated by the slow stratospheric transport, effectively causing the "age" of air masses to be higher than the tropospheric air below (Andrews et al., 2001). For N_2O, this effect is superimposed on the additional signal caused by its photo-chemical destruction in the stratosphere. No-

tably, during CoMet 1.0, two samples were collected with SF_6 ~~mixing ratios~~ mole fractions elevated by approximately 0.2 $\mathrm{pmol\,mol^{-1}}$. The first was filled on June 7th, at 9.2 km altitude, over Czechia, and second on June 12th, at 7.6 km, during the downward profile over the Po Valley. The potential source of these two observations might be worth investigating, especially in light of the constant atmospheric increase of the SF_6, despite substantial efforts to curb emissions of this potent greenhouse gas (Weiss and Prinn, 2011). Some attention was also given to molecular hydrogen (H_2) due to its potential feedbacks to the atmosphere oxidative capacity and stratospheric ozone levels (see Batenburg et al. (2012) and references therein). Values measured during the mission, namely 540 $\mathrm{nmol\,mol^{-1}}$ near the surface, approximately 550–560 $\mathrm{nmol\,mol^{-1}}$ throughout the free troposphere and ~~approx.~~ approximately 570 $\mathrm{nmol\,mol^{-1}}$ in the lower stratosphere, are comparable to previously reported values, e.g. in the scope of the CARIBIC project (Batenburg et al., 2012). This structure is driven by the presence of a relatively strong soil sink in the latitude band covered during CoMet 1.0, as has been confirmed by modelling studies (e.g. Pieterse et al., 2011). O_2/N_2 and Ar/N_2 ratios are presented for completeness, but are not discussed in the present study.

Of particular interest during CoMet 1.0 was the stable isotopic composition of methane. Abundances of both $\delta^{13}C-CH_4$ and $\delta^{2}H-CH_4$ are strongly and negatively correlated (R = -0.88 and R = -0.96, respectively) with ~~mixing ratios~~ mole fractions of methane, signifying the potential to use the isotopes as a marker of the source processes. Indeed, in the next section we present an application of using isotopic composition to differentiate between specific source types in the study area of the USCB.

3.6 Capturing the USCB source signature with isotopic data

Due to the broader spatial range covered by the HALO aircraft, the amount of samples taken over the USCB area using the JAS instrument was limited to 12 flasks, collected over two flights performed on May 29th and June 6th, 2018 (HALO flights 6 & 7, respectively). The main effort of flask sampling over USCB was carried out using another platform, namely FDLR Cessna (c.f. Fiehn et al., 2020, in review), aboard which a twin instrument was installed that allowed for a batch of approximately 60 samples to be collected, most of them inside the PBL. In the following paragraphs we only discuss samples collected on HALO. A broader discussion of methane isotopic composition observed during CoMet 1.0 will be a part of an upcoming study.

During flight 6 (Fig. 8, top left), the aircraft crossed the USCB at approximately 8 km altitude, then turned south-eastwards during the descent down to ca. 2 km, where it crossed into the PBL. Then, after turning south-westward, it crossed the USCB area upwind of the coal-mine sources at 1800 m, and, after another turn to north-west, it crossed the study area again, this time downwind of the known source locations. Along the flight path, 6 flasks were collected: two in the free troposphere during the high-altitude overpass and the descent, respectively, then two during the upwind crossing in the PBL and another two during the final downwind crossing inside the PBL. During flight 7 (Fig. 8, bottom left), a similar pattern was executed, with the exception that no upwind crossing in the PBL-section was executed. Again, two flasks were collected in the free troposphere immediately before and during the descent (at altitudes of 7.6 km and 4.3 km a.m.s.l., not shown on the plot), and four subsequent samples were collected during the PBL-section, flown at an altitude of 1400 m for the most part, until the aircraft was forced to ascend to ~~approx.~~ approximately 2 km after crossing into the airspace of Czechia.

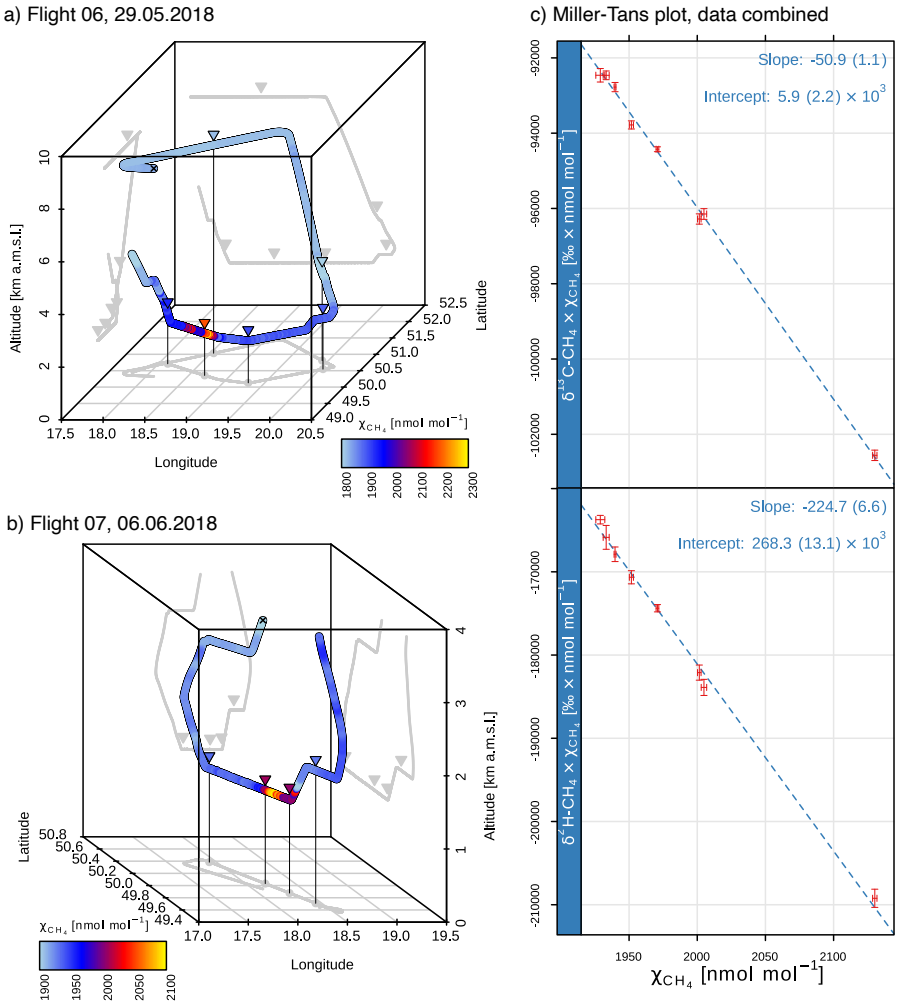

Figure 8. Left: Visualisation of CH_4 measurements over USCB during flights no. 6 (~~May 29th, top panel~~a) and no. 7 (~~June 6th, bottom panel~~b). For flight no. 7, only data from below 4 km altitude is plotted for clarity. Coloured lines represent ~~mixing ratios~~ mole fractions along the flight path~~. Triangles show~~ , with the ~~mean flask sampling point~~first plotted measurement marked with 'x', ~~coloured according to~~ triangles show the flask ~~mixing ratio~~sampling locations. Both in situ and flask ~~mixing ratios~~ mole fractions are coloured using the same scale. ~~Right:~~ c) Miller-Tans model of isotopic source signatures for δ^2H and $\delta^{13}C$, based on eight flask samples collected below 3 km over the USCB ~~. For flight~~ during flights no. 6 and 7 ~~only the four flask collected below 4 were included in the analysis~~together. See text description for details. The dashed line is the linear fit using the Williamson-York formula (Cantrell, 2008). Values of fit parameters are given with 1-σ uncertainty in the parentheses.

A comparison between patterns of in situ ~~mixing ratios~~ mole fractions and flask collection locations clearly shows that air masses with CH_4 ~~mixing ratios~~ mole fractions significantly enhanced by local sources were sampled at least three times. We have aggregated measurements from both days, assuming that the enhancement is coming from the same source (or source

cluster)~~on both days~~, which is partially corroborated by wind observations ~~on both days~~ (not shown) and modelling analyses supporting the campaign ~~(Nickl et al. and Gałkowski et al. , in prep).~~ (Nickl et al., 2020, Gałkowski et al., in prep). Application of the Miller-Tans approach (Fig. 8A) yields an isotopic signature for the USCB source of δ^2H = -224.7 (6.6) ‰ and δ^{13}C = -50.9 (1.1) ‰. Again, standard uncertainty in the final digits is given in brackets.

These values can be compared to previously published data. A comprehensive data set, gathering published values of isotopic signatures from various methane sources has been compiled and described by Sherwood et al. (2017). Most of the information it contains came from studies focused on methane emitted from fossil fuel extraction (including regular oil drilling, shale gas extraction as well as on gas emitted during coal mining), but data on biomass burning and biogenic sources is also included. Figure 9 shows the main ranges of these source signatures together with flask data collected during CoMet 1.0. Fossil-related methane sources are marked with rectangles (representing main ranges of the reported data and not their full extent) and biogenic source signatures as points (with bars marking the standard deviation of the reported signatures). As can be seen, the values reported in this study (marked with blue point with 1-σ ellipse) fall into the typical range reported in Sherwood et al. (2017), in the middle of conventional anthropogenic methane sources characterised by relatively high δ^2H (in contrast to the second cluster with δ^2H values closer to -300 ‰).

We also compared our results against signatures from the same area published previously. Measurements of methane, with samples collected in the coal mine tunnels, were performed by Kotarba (2001). Their study encompassed measurements of methane isotopic composition from a total of 15 mines in the USCB (with δ^2H measured in all but one), including samples collected from different coal seams. For the purpose of this study we have aggregated distinct samples reported in the original study and calculated mine-specific averages, which yielded the total range of δ^2H between -202.0 ‰ and -157.5 ‰. Reported values for δ^{13}C were between -77.1 ‰ and -44.5 ‰. These have been marked in Fig. 9 with a green rectangle labelled with "USCB".

In recent years there has also been a significant effort to constrain the USCB coal-mine source signatures, as many of the mines reported upon in Kotarba (2001) have been closed over the years, and those that remained open have completed the excavation of the old deposits and moved to different ones, possibly with different isotopic signatures. The results of these more recent measurements, representing methane emitted from 23 different coal-mine shafts, have yielded mean values of the signatures (δ^{13}C = -49.8 (5.7) ‰, δ^2H = -206.1 (46.3) ‰, brackets showing standard deviation), indicating that the methane emitted there has shifted to lower deuterium signatures (with almost unchanged values of δ^{13}C), corroborating the value reported in the present study. A more detailed discussion on these recent measurements will be presented in an upcoming study by Stanisavljevic et al. (in prep, this special issue).

4 Conclusions

A high-resolution in situ system for online observations of greenhouse gases (JIG) was successfully deployed during the CoMet 1.0 mission aboard the German research aircraft HALO aircraft over continental Europe. More than 55 hours of high frequency (1 Hz) observations of CO_2 and CH_4, and over 38 hours of CO observations were collected over the course of 9

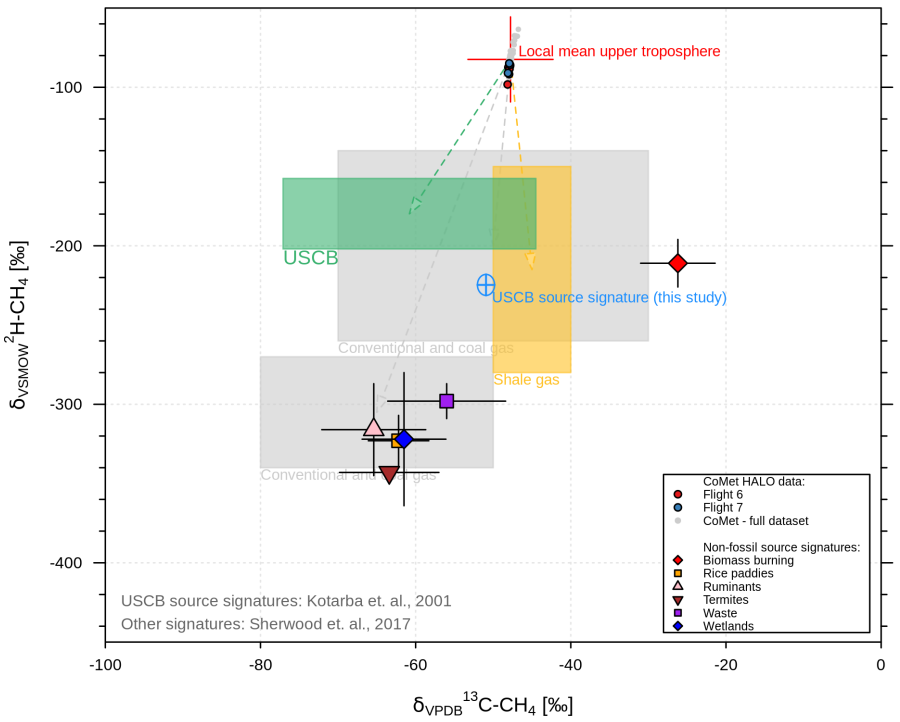

Figure 9. Isotopic composition of methane measured over the USCB (red and blue points) compared to source signatures estimated in this study using the Miller-Tans method (light blue cross with 1-σ uncertainty ellipsis), and previously reported ranges of isotopic composition for the dominant methane source groups. For the Miller-Tans method, the background signature was estimated using available measurements from the free troposphere (red cross). Data on global source signatures is based on Sherwood et al. (2017). Coloured blocks denote the approximate broad ranges of values reported there for a) coal and conventional gas excavation (purple), shale gas excavation (orange) and biomass burning (blue). Selected biogenic source signatures are also marked as points, with whiskers denoting the standard deviation of values reported in Sherwood et al. (2017). Data reported previously for USCB coal-mine sources by Kotarba (2001) is marked with a green rectangle.

flights between May 15th and June 12th, 2018. In addition to in situ observations, 96 discrete flask samples were collected and analysed for atmospheric composition, including δ^{13}C and δ^{2}H isotopic signatures of methane. Careful pre-flight, in-flight and post-flight calibration procedures allowed us to obtain a highly precise (single measurement standard deviations: 0.06 μmol mol^{-1} - CO_2, 0.3 nmol mol^{-1} - CH_4 and 3.1 nmol mol^{-1} - CO) data record that is traceable to international WMO calibration scales. Comparison with flask samples analysed in the laboratory confirm that the measurement data ~~comply~~ are close to compliance with the WMO compatibility goals (average bias smaller than 0.15 μmol mol-1 and 3 nmol mol^{-1} for CO_2 and CH_4, respectively).

Observations collected during the mission were used in combination with two of the available modelling products (CAMS and CarboScope) to explain the observed atmospheric variability on both regional scales as well as during the localised vertical soundings (a total of 50 throughout the campaign), covering altitudes from ground level to 14 km a.m.s.l.

Independent validation of available model products showed overall good agreement between observations and global state-of-the-art products, with very good agreement for $\mathrm{CH_4}$ and $\mathrm{CO_2}$ in the free troposphere / residual layer range (3–10 km) and slightly (CAMS) to significantly (CarboScope) worse performance in the PBL and the stratosphere. These results highlight i) the inability of the coarse-grid models to represent local sources and processes influencing individual profiles (in particular for CarboScope, but also clearly visible in the relatively high resolution CAMS product), and ii) challenges in the high-resolution modelling of biospheric fluxes of $\mathrm{CO_2}$.

We have also demonstrated the potential of using isotopic signatures measured in the downwind plume for source attribution. Samples collected during two flights above one of the main target areas of the CoMet 1.0 mission, the USCB, have clearly pointed to coal-mining as the main source of the observed methane enhancement ($\delta^{13}\mathrm{C}$ = -50.9 (1.1) ‰, $\delta^{2}\mathrm{H}$ = -224.7 (6.6) ‰). It should be noted that while the measured deuterium signatures are substantially lighter than has been reported in previous studies from the area, they correspond to more direct estimates performed in the scope of CoMet 1.0 by other involved teams (M. Stanisavljevic, personal communication), highlighting a shift in isotopic emission signatures following changes in coal-mining activities, e.g. the closure of coal mines or changes of excavated coal-beds/seams.

Code and data availability. The code used for data processing and analysis is available from the first author per request. The data collected during the mission are available on the HALO database at halo-db.pa.op.dlr.de

Author contributions. MG collected the data and prepared the manuscript, with contributions from all co-authors. SB, MR and AJ assisted with flask sample collection and performed the analyses. AA-P supplied CAMS model data and assisted with data interpretation. JM, FTK and JC contributed to the mission planning and data analysis. CG co-designed the CoMet 1.0 mission, collected the data and provided critical input to the manuscript.

Competing interests. The authors declare no competing interests.

Acknowledgements. We would like to express our appreciation to all the people involved in the CoMet campaign, without whom the campaign could not succeed. In particular we would like to thank DLR-FX for the campaign management, the pilots of the HALO aircraft, our colleagues at AGH University of Science and Technology and all the staff at MPI-BGC involved in the flask measurements. We also want to thank Mila Stanisavljevic for providing information on the isotopic composition in USCB. We gratefully acknowledge funding for the CoMet 1.0 campaign by MPG (Max Planck Society) and ~~by~~ BMBF (German Federal Ministry of Education and Research) through project

AIRSPACE (FK 390 01LK1701C), as well as German Research Foundation (Deutsche Forschungsgemeinschaft, DFG Priority Program SPP 1294). We also acknowledge the use of resources of Deutsches Klimarechnungszentrum (DKRZ), namely high-performance cluster Mistral, for data storage and analysis.

References

Agusti-Panareda, A., Diamantakis, M., Bayona, V., Klappenbach, F., and Butz, A.: Improving the inter-hemispheric gradient of total column atmospheric CO_2 and CH_4 in simulations with the ECMWF semi-Lagrangian atmospheric global model, Geoscientific Model Development, 10, 1–18, https://doi.org/10.5194/gmd-10-1-2017, https://www.geosci-model-dev.net/10/1/2017/, 2017.

Agustí-Panareda, A., Diamantakis, M., Massart, S., Chevallier, F., Muñoz Sabater, J., Barré, J., Curcoll, R., Engelen, R., Langerock, B., Law, R. M., Loh, Z., Morguí, J. A., Parrington, M., Peuch, V.-H., Ramonet, M., Roehl, C., Vermeulen, A. T., Warneke, T., and Wunch, D.: Modelling CO_2 weather – why horizontal resolution matters, Atmospheric Chemistry and Physics, 19, 7347–7376, https://doi.org/10.5194/acp-19-7347-2019, https://www.atmos-chem-phys.net/19/7347/2019/, 2019.

Ahmadov, R., Gerbig, C., Kretschmer, R., Koerner, S., Neininger, B., Dolman, A. J., and Sarrat, C.: Mesoscale covariance of transport and CO2 fluxes: Evidence from observations and simulations using the WRF-VPRM coupled atmosphere-biosphere model, Journal of Geophysical Research: Atmospheres, 112, https://doi.org/10.1029/2007JD008552, https://agupubs.onlinelibrary.wiley.com/doi/abs/10.1029/2007JD008552, 2007.

Amediek, A., Fix, A., Wirth, M., and Ehret, G.: Development of an OPO system at 1.57 micrometer for integrated path DIAL measurement of atmospheric carbon dioxide, Applied Physics B, 92, 295–302, https://doi.org/10.1007/s00340-008-3075-6, https://doi.org/10.1007/s00340-008-3075-6, 2008.

Amediek, A., Ehret, G., Fix, A., Wirth, M., Büdenbender, C., Quatrevalet, M., Kiemle, C., and Gerbig, C.: CHARM-F—a new airborne integrated-path differential-absorption lidar for carbon dioxide and methane observations: measurement performance and quantification of strong point source emissions, Appl. Opt., 56, 5182–5197, https://doi.org/10.1364/AO.56.005182, http://ao.osa.org/abstract.cfm?URI=ao-56-18-5182, 2017.

Andrews, A. E., Boering, K. A., Daube, B. C., Wofsy, S. C., Loewenstein, M., Jost, H., Podolske, J. R., Webster, C. R., Herman, R. L., Scott, D. C., Flesch, G. J., Moyer, E. J., Elkins, J. W., Dutton, G. S., Hurst, D. F., Moore, F. L., Ray, E. A., Romashkin, P. A., and Strahan, S. E.: Mean ages of stratospheric air derived from in situ observations of CO2, CH4, and N2O, Journal of Geophysical Research: Atmospheres, 106, 32 295–32 314, https://doi.org/10.1029/2001JD000465, https://agupubs.onlinelibrary.wiley.com/doi/abs/10.1029/2001JD000465, 2001.

Ballantyne, A. P., Andres, R., Houghton, R., Stocker, B. D., Wanninkhof, R., Anderegg, W., Cooper, L. A., DeGrandpre, M., Tans, P. P., Miller, J. B., Alden, C., and White, J. W. C.: Audit of the global carbon budget: estimate errors and their impact on uptake uncertainty, Biogeosciences, 12, 2565–2584, https://doi.org/10.5194/bg-12-2565-2015, https://www.biogeosciences.net/12/2565/2015/, 2015.

Basu, S., Guerlet, S., Butz, A., Houweling, S., Hasekamp, O., Aben, I., Krummel, P., Steele, P., Langenfelds, R., Torn, M., Biraud, S., Stephens, B., Andrews, A., and Worthy, D.: Global CO_2 fluxes estimated from GOSAT retrievals of total column CO_2, Atmospheric Chemistry and Physics, 13, 8695–8717, https://doi.org/10.5194/acp-13-8695-2013, https://www.atmos-chem-phys.net/13/8695/2013/, 2013.

Batenburg, A. M., Schuck, T. J., Baker, A. K., Zahn, A., Brenninkmeijer, C. A. M., and Röckmann, T.: The stable isotopic composition of molecular hydrogen in the tropopause region probed by the CARIBIC aircraft, Atmospheric Chemistry and Physics, 12, 4633–4646, https://doi.org/10.5194/acp-12-4633-2012, https://www.atmos-chem-phys.net/12/4633/2012/, 2012.

Bergamaschi, P., Houweling, S., Segers, A., Krol, M., Frankenberg, C., Scheepmaker, R. A., Dlugokencky, E., Wofsy, S. C., Kort, E. A., Sweeney, C., Schuck, T., Brenninkmeijer, C., Chen, H., Beck, V., and Gerbig, C.: Atmospheric CH4 in the first decade of the 21st century: Inverse modeling analysis using SCIAMACHY satellite retrievals and NOAA surface measurements, Journal of Geophysical Research:

Atmospheres, 118, 7350–7369, https://doi.org/10.1002/jgrd.50480, https://agupubs.onlinelibrary.wiley.com/doi/abs/10.1002/jgrd.50480, 2013.

Bergamaschi, P., Danila, A., Weiss, R. F., Ciais, P., Thompson, R. L., Brunner, D., Levin, I., Meijer, Y., Chevallier, F., Janssens-Maenhout, G., Bovensmann, H., Crisp, D., Basu, S., Dlugokencky, E., Engelen, R., Gerbig, C., Günther, D., Hammer, S., Henne, S., Houweling, S., Karstens, U., Kort, E., Maione, M., Manning, A. J., Miller, J., Montzka, S., Pandey, S., Peters, W., Peylin, P., Pinty, B., Ramonet, M., Reimann, S., Röckmann, T., Schmidt, M., Strogies, M., Sussams, J., Tarasova, O., van Aardenne, J., Vermeulen, A. T., and Vogel, F.: Atmospheric monitoring and inverse modelling for verification of greenhouse gas inventories, Tech. Rep. ISBN 978-92-79-88938-7, doi:10.2760/759928, JRC111789, JRC, Publications Office of the European Union, Luxembourg, 2018.

Boschetti, F., Chen, H., Thouret, V., Nedelec, P., Janssens-Maenhout, G., and Gerbig, C.: On the representation of IAGOS/MOZAIC vertical profiles in chemical transport models: contribution of different error sources in the example of carbon monoxide, Tellus B: Chemical and Physical Meteorology, 67, 28 292, https://doi.org/10.3402/tellusb.v67.28292, https://doi.org/10.3402/tellusb.v67.28292, 2015.

Boschetti, F., Thouret, V., Maenhout, G. J., Totsche, K. U., Marshall, J., and Gerbig, C.: Multi-species inversion and IAGOS airborne data for a better constraint of continental-scale fluxes, Atmospheric Chemistry and Physics, 18, 9225–9241, https://doi.org/10.5194/acp-18-9225-2018, https://www.atmos-chem-phys.net/18/9225/2018/, 2018.

Bovensmann, H., Burrows, J. P., Buchwitz, M., Frerick, J., Noël, S., Rozanov, V. V., Chance, K. V., and Goede, A. P. H.: SCIAMACHY: Mission Objectives and Measurement Modes, Journal of the Atmospheric Sciences, 56, 127–150, https://doi.org/10.1175/1520-0469(1999)056<0127:SMOAMM>2.0.CO;2, https://doi.org/10.1175/1520-0469(1999)056<0127:SMOAMM>2.0.CO;2, 1999.

Butz, A., Galli, A., Hasekamp, O., Landgraf, J., Tol, P., and Aben, I.: TROPOMI aboard Sentinel-5 Precursor: Prospective performance of CH4 retrievals for aerosol and cirrus loaded atmospheres, Remote Sensing of Environment, 120, 267 – 276, https://doi.org/https://doi.org/10.1016/j.rse.2011.05.030, http://www.sciencedirect.com/science/article/pii/S003442571200082X, the Sentinel Missions - New Opportunities for Science, 2012.

Cambaliza, M. O. L., Shepson, P. B., Caulton, D. R., Stirm, B., Samarov, D., Gurney, K. R., Turnbull, J., Davis, K. J., Possolo, A., Karion, A., Sweeney, C., Moser, B., Hendricks, A., Lauvaux, T., Mays, K., Whetstone, J., Huang, J., Razlivanov, I., Miles, N. L., and Richardson, S. J.: Assessment of uncertainties of an aircraft-based mass balance approach for quantifying urban greenhouse gas emissions, Atmospheric Chemistry and Physics, 14, 9029–9050, https://doi.org/10.5194/acp-14-9029-2014, https://www.atmos-chem-phys.net/14/9029/2014/, 2014.

Cantrell, C. A.: Technical Note: Review of methods for linear least-squares fitting of data and application to atmospheric chemistry problems, Atmospheric Chemistry and Physics, 8, 5477–5487, https://doi.org/10.5194/acp-8-5477-2008, https://www.atmos-chem-phys.net/8/5477/2008/, 2008.

Chen, H., Winderlich, J., Gerbig, C., Hoefer, A., Rella, C. W., Crosson, E. R., Van Pelt, A. D., Steinbach, J., Kolle, O., Beck, V., Daube, B. C., Gottlieb, E. W., Chow, V. Y., Santoni, G. W., and Wofsy, S. C.: High-accuracy continuous airborne measurements of greenhouse gases (CO_2 and CH_4) using the cavity ring-down spectroscopy (CRDS) technique, Atmospheric Measurement Techniques, 3, 375–386, https://doi.org/10.5194/amt-3-375-2010, https://www.atmos-meas-tech.net/3/375/2010/, 2010.

Chen, H., Winderlich, J., Gerbig, C., Katrynski, K., Jordan, A., and Heimann, M.: Validation of routine continuous airborne CO_2 observations near the Bialystok Tall Tower, Atmospheric Measurement Techniques, 5, 873–889, https://doi.org/10.5194/amt-5-873-2012, https://www.atmos-meas-tech.net/5/873/2012/, 2012.

Ciais, P., Dolman, A. J., Bombelli, A., Duren, R., Peregon, A., Rayner, P. J., Miller, C., Gobron, N., Kinderman, G., Marland, G., Gruber, N., Chevallier, F., Andres, R. J., Balsamo, G., Bopp, L., Bréon, F.-M., Broquet, G., Dargaville, R., Battin, T. J., Borges, A., Bovensmann, H.,

Buchwitz, M., Butler, J., Canadell, J. G., Cook, R. B., DeFries, R., Engelen, R., Gurney, K. R., Heinze, C., Heimann, M., Held, A., Henry, M., Law, B., Luyssaert, S., Miller, J., Moriyama, T., Moulin, C., Myneni, R. B., Nussli, C., Obersteiner, M., Ojima, D., Pan, Y., Paris, J.-D., Piao, S. L., Poulter, B., Plummer, S., Quegan, S., Raymond, P., Reichstein, M., Rivier, L., Sabine, C., Schimel, D., Tarasova, O., Valentini, R., Wang, R., van der Werf, G., Wickland, D., Williams, M., and Zehner, C.: Current systematic carbon-cycle observations and the need for implementing a policy-relevant carbon observing system, Biogeosciences, 11, 3547–3602, https://doi.org/10.5194/bg-11-3547-2014, https://www.biogeosciences.net/11/3547/2014/, 2014.

Dobler, J. T., Harrison, F. W., Browell, E. V., Lin, B., McGregor, D., Kooi, S., Choi, Y., and Ismail, S.: Atmospheric CO2 column measurements with an airborne intensity-modulated continuous wave 1.57 μm fiber laser lidar, Appl. Opt., 52, 2874–2892, https://doi.org/10.1364/AO.52.002874, http://ao.osa.org/abstract.cfm?URI=ao-52-12-2874, 2013.

Du, J., Sun, Y., Chen, D., Mu, Y., Huang, M., Yang, Z., Liu, J., Bi, D., Hou, X., and Chen, W.: Frequency-stabilized laser system at 1572 nm for space-borne CO 2 detection LIDAR, Chinese Optics Letters, 15, 031 401, 2017.

E-PRTR: E-PRTR, v16, Website, https://www.eea.europa.eu/ds_resolveuid/64dbc8e60ce4411f94ac25e9bd961ee4, 2019.

Eldering, A., Boland, S., Solish, B., Crisp, D., Kahn, P., and Gunson, M.: High precision atmospheric CO2 measurements from space: The design and implementation of OCO-2, in: 2012 IEEE Aerospace Conference, pp. 1–10, https://doi.org/10.1109/AERO.2012.6187176, 2012.

Fiehn, A., Kostinek, J., Eckl, M., Klausner, T., Gałkowski, M., Chen, J., Gerbig, C., Röckmann, T., Maazallahi, H., Schmidt, M., Korbeń, P., Nęcki, J., Jagoda, P., Wildmann, N., Mallaun, C., Bun, R., Nickl, A.-L., Jöckel, P., Fix, A., and Roiger, A.: Estimating CH_4, CO_2, and CO emissions from coal mining and industrial activities in the Upper Silesian Coal Basin using an aircraft-based mass balance approach, Atmospheric Chemistry and Physics Discussions, 2020, 1–33, https://doi.org/10.5194/acp-2020-282, https://www.atmos-chem-phys-discuss.net/acp-2020-282/, 2020.

Filges, A., Gerbig, C., Chen, H., Franke, H., Klaus, C., and Jordan, A.: The IAGOS-core greenhouse gas package: a measurement system for continuous airborne observations of CO2, CH4, H2O and CO, Tellus B: Chemical and Physical Meteorology, 67, 27 989, https://doi.org/10.3402/tellusb.v67.27989, https://doi.org/10.3402/tellusb.v67.27989, 2015.

Filges, A., Gerbig, C., Rella, C. W., Hoffnagle, J., Smit, H., Krämer, M., Spelten, N., Rolf, C., Bozóki, Z., Buchholz, B., and Ebert, V.: Evaluation of the IAGOS-Core GHG package H_2O measurements during the DENCHAR airborne inter-comparison campaign in 2011, Atmospheric Measurement Techniques, 11, 5279–5297, https://doi.org/10.5194/amt-11-5279-2018, https://www.atmos-meas-tech.net/11/5279/2018/, 2018.

Geibel, M. C., Messerschmidt, J., Gerbig, C., Blumenstock, T., Chen, H., Hase, F., Kolle, O., Lavrič, J. V., Notholt, J., Palm, M., Rettinger, M., Schmidt, M., Sussmann, R., Warneke, T., and Feist, D. G.: Calibration of column-averaged CH_4 over European TCCON FTS sites with airborne in-situ measurements, Atmospheric Chemistry and Physics, 12, 8763–8775, https://doi.org/10.5194/acp-12-8763-2012, https://www.atmos-chem-phys.net/12/8763/2012/, 2012.

Gerilowski, K., Tretner, A., Krings, T., Buchwitz, M., Bertagnolio, P. P., Belemezov, F., Erzinger, J., Burrows, J. P., and Bovensmann, H.: MAMAP – a new spectrometer system for column-averaged methane and carbon dioxide observations from aircraft: instrument description and performance analysis, Atmospheric Measurement Techniques, 4, 215–243, https://doi.org/10.5194/amt-4-215-2011, https://www.atmos-meas-tech.net/4/215/2011/, 2011.

Heimann, M. and Körner, S.: The Global Atmospheric Tracer Model TM3, Max Planck Institute for Biogeochemistry, Hans-Knöll Str. 10, 07745 Jena, 2003.

Hughes, R. and Jiang, B.: The permeabilities of carbon dioxide, nitrous oxide and oxygen and their mixtures through silicone rubber and cellulose acetate membranes, Gas Separation and Purification, 9, 27 – 30, https://doi.org/https://doi.org/10.1016/0950-4214(95)92173-A, http://www.sciencedirect.com/science/article/pii/095042149592173A, 1995.

Inness, A., Blechschmidt, A.-M., Bouarar, I., Chabrillat, S., Crepulja, M., Engelen, R. J., Eskes, H., Flemming, J., Gaudel, A., Hendrick, F., Huijnen, V., Jones, L., Kapsomenakis, J., Katragkou, E., Keppens, A., Langerock, B., de Mazière, M., Melas, D., Parrington, M., Peuch, V. H., Razinger, M., Richter, A., Schultz, M. G., Suttie, M., Thouret, V., Vrekoussis, M., Wagner, A., and Zerefos, C.: Data assimilation of satellite-retrieved ozone, carbon monoxide and nitrogen dioxide with ECMWF's Composition-IFS, Atmospheric Chemistry and Physics, 15, 5275–5303, https://doi.org/10.5194/acp-15-5275-2015, https://www.atmos-chem-phys.net/15/5275/2015/, 2015.

Inness, A., Ades, M., Agustí-Panareda, A., Barré, J., Benedictow, A., Blechschmidt, A.-M., Dominguez, J. J., Engelen, R., Eskes, H., Flemming, J., Huijnen, V., Jones, L., Kipling, Z., Massart, S., Parrington, M., Peuch, V.-H., Razinger, M., Remy, S., Schulz, M., and Suttie, M.: The CAMS reanalysis of atmospheric composition, Atmospheric Chemistry and Physics, 19, 3515–3556, https://doi.org/10.5194/acp-19-3515-2019, https://www.atmos-chem-phys.net/19/3515/2019/, 2019.

IPCC, (eds.) Stocker, T., Qin, D., Plattner, G.-K., Tignor, M., Allen, S., Boschung, J., Nauels, A., Xia, Y., Bex, V., and Midgley, P.: Climate Change 2013: The Physical Science Basis. Contribution of Working Group I to the Fifth Assessment Report of the Intergovernmental Panel on Climate Change, Cambridge University Press, Cambridge, United Kingdom and New York, NY, USA, 2013.

JCGM: Evaluation of measurement data — Guide to the expression of uncertainty in measurement, JCGM (EC, IFCC, ILAC, ISO, IUPAC, IUPAP, OIML and BIPM), 2008.

Karion, A., Sweeney, C., Pétron, G., Frost, G., Michael Hardesty, R., Kofler, J., Miller, B. R., Newberger, T., Wolter, S., Banta, R., Brewer, A., Dlugokencky, E., Lang, P., Montzka, S. A., Schnell, R., Tans, P., Trainer, M., Zamora, R., and Conley, S.: Methane emissions estimate from airborne measurements over a western United States natural gas field, Geophysical Research Letters, 40, 4393–4397, https://doi.org/10.1002/grl.50811, https://agupubs.onlinelibrary.wiley.com/doi/abs/10.1002/grl.50811, 2013a.

Karion, A., Sweeney, C., Wolter, S., Newberger, T., Chen, H., Andrews, A., Kofler, J., Neff, D., and Tans, P.: Long-term greenhouse gas measurements from aircraft, Atmospheric Measurement Techniques, 6, 511–526, https://doi.org/10.5194/amt-6-511-2013, https://amt.copernicus.org/articles/6/511/2013/, 2013b.

Keeling, C. D.: The concentration and isotopic abundances of atmospheric carbon dioxide in rural areas, Geochimica et Cosmochimica Acta, 13, 322 – 334, https://doi.org/https://doi.org/10.1016/0016-7037(58)90033-4, http://www.sciencedirect.com/science/article/pii/0016703758900334, 1958.

Kirschke, S., Bousquet, P., Ciais, P., Saunois, M., Canadell, J. G., Dlugokencky, E. J., Bergamaschi, P., Bergmann, D., Blake, D. R., Bruhwiler, L., Cameron-Smith, P., Castaldi, S., Chevallier, F., Feng, L., Fraser, A., Heimann, M., Hodson, E. L., Houweling, S., Josse, B., Fraser, P. J., Krummel, P. B., Lamarque, J.-F., Langenfelds, R. L., Le Quéré, C., Naik, V., O'Doherty, S., Palmer, P. I., Pison, I., Plummer, D., Poulter, B., Prinn, R. G., Rigby, M., Ringeval, B., Santini, M., Schmidt, M., Shindell, D. T., Simpson, I. J., Spahni, R., Steele, L. P., Strode, S. A., Sudo, K., Szopa, S., van der Werf, G. R., Voulgarakis, A., van Weele, M., Weiss, R. F., Williams, J. E., and Zeng, G.: Three decades of global methane sources and sinks, Nature Geoscience, 6, 813–823, https://doi.org/10.1038/ngeo1955, https://doi.org/10.1038/ngeo1955, 2013.

Kotarba, M. J.: Composition and origin of coalbed gases in the Upper Silesian and Lublin basins, Poland, Organic Geochemistry, 32, 163 – 180, https://doi.org/https://doi.org/10.1016/S0146-6380(00)00134-0, http://www.sciencedirect.com/science/article/pii/S0146638000001340, 2001.

Krings, T., Gerilowski, K., Buchwitz, M., Hartmann, J., Sachs, T., Erzinger, J., Burrows, J. P., and Bovensmann, H.: Quantification of methane emission rates from coal mine ventilation shafts using airborne remote sensing data, Atmospheric Measurement Techniques, 6, 151–166, https://doi.org/10.5194/amt-6-151-2013, https://www.atmos-meas-tech.net/6/151/2013/, 2013.

Kuze, A., Suto, H., Nakajima, M., and Hamazaki, T.: Thermal and near infrared sensor for carbon observation Fourier-transform spectrometer on the Greenhouse Gases Observing Satellite for greenhouse gases monitoring, Appl. Opt., 48, 6716–6733, https://doi.org/10.1364/AO.48.006716, http://ao.osa.org/abstract.cfm?URI=ao-48-35-6716, 2009.

Le Quéré, C., Andrew, R. M., Friedlingstein, P., Sitch, S., Hauck, J., Pongratz, J., Pickers, P. A., Korsbakken, J. I., Peters, G. P., Canadell, J. G., Arneth, A., Arora, V. K., Barbero, L., Bastos, A., Bopp, L., Chevallier, F., Chini, L. P., Ciais, P., Doney, S. C., Gkritzalis, T., Goll, D. S., Harris, I., Haverd, V., Hoffman, F. M., Hoppema, M., Houghton, R. A., Hurtt, G., Ilyina, T., Jain, A. K., Johannessen, T., Jones, C. D., Kato, E., Keeling, R. F., Goldewijk, K. K., Landschützer, P., Lefèvre, N., Lienert, S., Liu, Z., Lombardozzi, D., Metzl, N., Munro, D. R., Nabel, J. E. M. S., Nakaoka, S., Neill, C., Olsen, A., Ono, T., Patra, P., Peregon, A., Peters, W., Peylin, P., Pfeil, B., Pierrot, D., Poulter, B., Rehder, G., Resplandy, L., Robertson, E., Rocher, M., Rödenbeck, C., Schuster, U., Schwinger, J., Séférian, R., Skjelvan, I., Steinhoff, T., Sutton, A., Tans, P. P., Tian, H., Tilbrook, B., Tubiello, F. N., van der Laan-Luijkx, I. T., van der Werf, G. R., Viovy, N., Walker, A. P., Wiltshire, A. J., Wright, R., Zaehle, S., and Zheng, B.: Global Carbon Budget 2018, Earth System Science Data, 10, 2141–2194, https://doi.org/10.5194/essd-10-2141-2018, https://www.earth-syst-sci-data.net/10/2141/2018/, 2018.

Leifer, I., Melton, C., Fischer, M. L., Fladeland, M., Frash, J., Gore, W., Iraci, L. T., Marrero, J. E., Ryoo, J.-M., Tanaka, T., and Yates, E. L.: Atmospheric characterization through fused mobile airborne and surface in situ surveys: methane emissions quantification from a producing oil field, Atmospheric Measurement Techniques, 11, 1689–1705, https://doi.org/10.5194/amt-11-1689-2018, https://www.atmos-meas-tech.net/11/1689/2018/, 2018.

Massart, S., Agusti-Panareda, A., Aben, I., Butz, A., Chevallier, F., Crevoisier, C., Engelen, R., Frankenberg, C., and Hasekamp, O.: Assimilation of atmospheric methane products into the MACC-II system: from SCIAMACHY to TANSO and IASI, Atmospheric Chemistry and Physics, 14, 6139–6158, https://doi.org/10.5194/acp-14-6139-2014, https://www.atmos-chem-phys.net/14/6139/2014/, 2014.

Massart, S., Agustí-Panareda, A., Heymann, J., Buchwitz, M., Chevallier, F., Reuter, M., Hilker, M., Burrows, J. P., Deutscher, N. M., Feist, D. G., Hase, F., Sussmann, R., Desmet, F., Dubey, M. K., Griffith, D. W. T., Kivi, R., Petri, C., Schneider, M., and Velazco, V. A.: Ability of the 4-D-Var analysis of the GOSAT BESD XCO_2 retrievals to characterize atmospheric CO_2 at large and synoptic scales, Atmospheric Chemistry and Physics, 16, 1653–1671, https://doi.org/10.5194/acp-16-1653-2016, https://www.atmos-chem-phys.net/16/1653/2016/, 2016.

Miller, J. B. and Tans, P. P.: Calculating isotopic fractionation from atmospheric measurements at various scales, Tellus B, 55, 207–214, https://doi.org/10.1034/j.1600-0889.2003.00020.x, https://onlinelibrary.wiley.com/doi/abs/10.1034/j.1600-0889.2003.00020.x, 2003.

Nickl, A.-L., Mertens, M., Roiger, A., Fix, A., Amediek, A., Fiehn, A., Gerbig, C., Galkowski, M., Kerkweg, A., Klausner, T., Eckl, M., and Jöckel, P.: Hindcasting and forecasting of regional methane from coal mine emissions in the Upper Silesian Coal Basin using the online nested global regional chemistry–climate model MECO(n) (MESSy v2.53), Geoscientific Model Development, 13, 1925–1943, https://doi.org/10.5194/gmd-13-1925-2020, https://gmd.copernicus.org/articles/13/1925/2020/, 2020.

Nisbet, E. G., Manning, M. R., Dlugokencky, E. J., Fisher, R. E., Lowry, D., Michel, S. E., Myhre, C. L., Platt, S. M., Allen, G., Bousquet, P., Brownlow, R., Cain, M., France, J. L., Hermansen, O., Hossaini, R., Jones, A. E., Levin, I., Manning, A. C., Myhre, G., Pyle, J. A., Vaughn, B. H., Warwick, N. J., and White, J. W. C.: Very Strong Atmospheric Methane Growth in the 4 Years 2014–2017: Implications for the Paris Agreement, Global Biogeochemical Cycles, 33, 318–342, https://doi.org/10.1029/2018GB006009, https://agupubs.onlinelibrary.wiley.com/doi/abs/10.1029/2018GB006009, 2019.

NOAA: Trends in Atmospheric Methane, https://esrl.noaa.gov/gmd/ccgg/trends_ch4/, 2020.

Park, C., Gerbig, C., Newman, S., Ahmadov, R., Feng, S., Gurney, K. R., Carmichael, G. R., Park, S.-Y., Lee, H.-W., Goulden, M., Stutz, J., Peischl, J., and Ryerson, T.: CO2 Transport, Variability, and Budget over the Southern California Air Basin Using the High-Resolution WRF-VPRM Model during the CalNex 2010 Campaign, Journal of Applied Meteorology and Climatology, 57, 1337–1352, https://doi.org/10.1175/JAMC-D-17-0358.1, https://doi.org/10.1175/JAMC-D-17-0358.1, 2018.

Pieterse, G., Krol, M. C., Batenburg, A. M., Steele, L. P., Krummel, P. B., Langenfelds, R. L., and Röckmann, T.: Global modelling of H_2 mixing ratios and isotopic compositions with the TM5 model, Atmospheric Chemistry and Physics, 11, 7001–7026, https://doi.org/10.5194/acp-11-7001-2011, https://www.atmos-chem-phys.net/11/7001/2011/, 2011.

Reum, F., Gerbig, C., Lavric, J. V., Rella, C. W., and Göckede, M.: Correcting atmospheric CO_2 and CH_4 mole fractions obtained with Picarro analyzers for sensitivity of cavity pressure to water vapor, Atmospheric Measurement Techniques, 12, 1013–1027, https://doi.org/10.5194/amt-12-1013-2019, https://www.atmos-meas-tech.net/12/1013/2019/, 2019.

Reuter, M., Bovensmann, H., Buchwitz, M., Burrows, J. P., Connor, B. J., Deutscher, N. M., Griffith, D. W. T., Heymann, J., Keppel-Aleks, G., Messerschmidt, J., Notholt, J., Petri, C., Robinson, J., Schneising, O., Sherlock, V., Velazco, V., Warneke, T., Wennberg, P. O., and Wunch, D.: Retrieval of atmospheric CO2 with enhanced accuracy and precision from SCIAMACHY: Validation with FTS measurements and comparison with model results, Journal of Geophysical Research: Atmospheres, 116, https://doi.org/10.1029/2010JD015047, https://agupubs.onlinelibrary.wiley.com/doi/abs/10.1029/2010JD015047, 2011.

Reuter, M., Buchwitz, M., Schneising, O., Krautwurst, S., O'Dell, C. W., Richter, A., Bovensmann, H., and Burrows, J. P.: Towards monitoring localized CO_2 emissions from space: co-located regional CO_2 and NO_2 enhancements observed by the OCO-2 and S5P satellites, Atmospheric Chemistry and Physics, 19, 9371–9383, https://doi.org/10.5194/acp-19-9371-2019, https://www.atmos-chem-phys.net/19/9371/2019/, 2019.

Röckmann, T., Eyer, S., van der Veen, C., Popa, M. E., Tuzson, B., Monteil, G., Houweling, S., Harris, E., Brunner, D., Fischer, H., Zazzeri, G., Lowry, D., Nisbet, E. G., Brand, W. A., Necki, J. M., Emmenegger, L., and Mohn, J.: In situ observations of the isotopic composition of methane at the Cabauw tall tower site, Atmospheric Chemistry and Physics, 16, 10 469–10 487, https://doi.org/10.5194/acp-16-10469-2016, https://www.atmos-chem-phys.net/16/10469/2016/, 2016.

Rödenbeck, C.: Estimating CO_2 sources and sinks from atmospheric mixing ratio measurements using a global inversion of atmospheric transport, Technical report 6, Max Planck Institute for Biogeochemistry, 2005.

Rödenbeck, C., Houweling, S., Gloor, M., and Heimann, M.: CO_2 flux history 1982–2001 inferred from atmospheric data using a global inversion of atmospheric transport, Atmospheric Chemistry and Physics, 3, 1919–1964, https://doi.org/10.5194/acp-3-1919-2003, https://www.atmos-chem-phys.net/3/1919/2003/, 2003.

Saeki, T., Maksyutov, S., Sasakawa, M., Machida, T., Arshinov, M., Tans, P., Conway, T. J., Saito, M., Valsala, V., Oda, T., Andres, R. J., and Belikov, D.: Carbon flux estimation for Siberia by inverse modeling constrained by aircraft and tower CO2 measurements, Journal of Geophysical Research: Atmospheres, 118, 1100–1122, https://doi.org/10.1002/jgrd.50127, https://agupubs.onlinelibrary.wiley.com/doi/abs/10.1002/jgrd.50127, 2013.

Sakaizawa, D., Nagasawa, C., Nagai, T., Abo, M., Shibata, Y., Nakazato, M., and Sakai, T.: Development of a 1.6 μm differential absorption lidar with a quasi-phase-matching optical parametric oscillator and photon-counting detector for the vertical CO 2 profile, Applied optics, 48, 748–757, 2009.

Sarrat, C., Noilhan, J., Lacarrère, P., Donier, S., Lac, C., Calvet, J. C., Dolman, A. J., Gerbig, C., Neininger, B., Ciais, P., Paris, J. D., Boumard, F., Ramonet, M., and Butet, A.: Atmospheric CO2 modeling at the regional scale: Application to the CarboEurope Regional

Experiment, Journal of Geophysical Research: Atmospheres, 112, https://doi.org/10.1029/2006JD008107, https://agupubs.onlinelibrary.wiley.com/doi/abs/10.1029/2006JD008107, 2007.

Sherwood, O. A., Schwietzke, S., Arling, V. A., and Etiope, G.: Global Inventory of Gas Geochemistry Data from Fossil Fuel, Microbial and Burning Sources, version 2017, Earth System Science Data, 9, 639–656, https://doi.org/10.5194/essd-9-639-2017, https://www.earth-syst-sci-data.net/9/639/2017/, 2017.

Sperlich, P., Uitslag, N. A. M., Richter, J. M., Rothe, M., Geilmann, H., van der Veen, C., Röckmann, T., Blunier, T., and Brand, W. A.: Development and evaluation of a suite of isotope reference gases
for methane in air, Atmospheric Measurement Techniques, 9, 3717–3737, https://doi.org/10.5194/amt-9-3717-2016, https://www.atmos-meas-tech.net/9/3717/2016/, 2016.

Spiers, G. D., Menzies, R. T., Jacob, J., Christensen, L. E., Phillips, M. W., Choi, Y., and Browell, E. V.: Atmospheric CO2 measurements with a 2 micrometer airborne laser absorption spectrometer employing coherent detection., Appl Opt, 50, 2098–2111, https://doi.org/10.1364/AO.50.002098, 2011.

Sweeney, C., Karion, A., Wolter, S., Newberger, T., Guenther, D., Higgs, J. A., Andrews, A. E., Lang, P. M., Neff, D., Dlugokencky, E., Miller, J. B., Montzka, S. A., Miller, B. R., Masarie, K. A., Biraud, S. C., Novelli, P. C., Crotwell, M., Crotwell, A. M., Thoning, K., and Tans, P. P.: Seasonal climatology of CO2 across North America from aircraft measurements in the NOAA/ESRL Global Greenhouse Gas Reference Network, Journal of Geophysical Research: Atmospheres, 120, 5155–5190, https://doi.org/10.1002/2014JD022591, https://agupubs.onlinelibrary.wiley.com/doi/abs/10.1002/2014JD022591, 2015.

Umezawa, T., Matsueda, H., Sawa, Y., Niwa, Y., Machida, T., and Zhou, L.: Seasonal evaluation of tropospheric CO_2 over the Asia-Pacific region observed by the CONTRAIL commercial airliner measurements, Atmospheric Chemistry and Physics, 18, 14 851–14 866, https://doi.org/10.5194/acp-18-14851-2018, https://www.atmos-chem-phys.net/18/14851/2018/, 2018.

Varon, D. J., Jacob, D. J., McKeever, J., Jervis, D., Durak, B. O. A., Xia, Y., and Huang, Y.: Quantifying methane point sources from fine-scale satellite observations of atmospheric methane plumes, Atmospheric Measurement Techniques, 11, 5673–5686, https://doi.org/10.5194/amt-11-5673-2018, https://www.atmos-meas-tech.net/11/5673/2018/, 2018.

Verma, S., Marshall, J., Parrington, M., Agustí-Panareda, A., Massart, S., Chipperfield, M. P., Wilson, C., and Gerbig, C.: Extending methane profiles from aircraft into the stratosphere for satellite total column validation using the ECMWF C-IFS and TOMCAT/SLIMCAT 3-D model, Atmospheric Chemistry and Physics, 17, 6663–6678, https://doi.org/10.5194/acp-17-6663-2017, https://www.atmos-chem-phys.net/17/6663/2017/, 2017.

Weiss, R. F. and Prinn, R. G.: Quantifying greenhouse-gas emissions from atmospheric measurements: a critical reality check for climate legislation, Philosophical Transactions of the Royal Society A: Mathematical, Physical and Engineering Sciences, 369, 1925–1942, 2011.

WMO: 20th WMO/IAEA Meeting on Carbon Dioxide, Other Greenhouse Gases and Related Measurement Techniques (GGMT-2019), GAW Report No. 255, 2019.

Wofsy, S. C.: HIAPER Pole-to-Pole Observations (HIPPO): fine-grained, global-scale measurements of climatically important atmospheric gases and aerosols, Philosophical Transactions of the Royal Society A: Mathematical, Physical and Engineering Sciences, 369, 2073–2086, 2011.